GEOLOGY OF A SECTION OF IGNIMBRITES

NEAR SACRAMENTO, CHIHUAHUA, MEXICO

by

Daniel G. Gall

APPROVED BY:

THESIS COMMITTEE

Richard L. Mauger

Dr. Richard L. Mauger, Supervising Professor

B. A. Bishop

Dr. B. A. Bishop

Pei-lin Tien

Dr. Pei-lin Tien

S Schamel

Dr. Steven Schamel

CHAIRMAN OF THE DEPARTMENT OF GEOLOGY

Michael P. O'Connor

Dr. Michael P. O'Connor

DEAN OF THE GRADUATE SCHOOL

Joseph G. Boyette

Dr. Joseph G. Boyette

GEOLOGY OF A SECTION OF IGNIMBRITES NEAR SACRAMENTO, CHIHUAHUA, MEXICO

A Thesis

Presented to

the Faculty of the Department of Geology

East Carolina University

In Partial Fulfillment

of the Requirements for the Degree

Master of Science in Geology

by

Daniel G. Gall

January 1977

GEOLOGY OF A SECTION OF IGNIMBRITES NEAR SACRAMENTO, CHIHUAHUA, MEXICO

by

Daniel G. Gall

A B S T R A C T

A sequence of rhyolitic ignimbrites, 150 m in thickness, is exposed along the southern edge of the Rio Sacramento flood plain approximately 25 km northwest of Chihuahua, Chihuahua, Mexico (long. 106° 12.2' W and lat. 28° 50.8' N). These rocks dip 15° NE and conform to the general low eastward dips of the late Eocene rhyolites between Majalca and Chihuahua City.

The ignimbrites include welded vitric tuffs (Units 1, 2, 3, and 5) and a welded lithic tuff (Unit 4). Unit 1 is a single flow and cooling unit. Units 2, 3, and 4 comprise a multiple-flow, single cooling unit. Unit 5 is a single flow and cooling unit. Sanidine is the predominant phenocryst (Or_{40-70}). Minor amounts of plagioclase (An_{29}) and quartz phenocrysts are also present. The groundmass of the ignimbrites consists of sanidine and SiO_2 polymorphs. The ignimbrites are classified as alkali rhyolites because of the predominance of sanidine and SiO_2. The welded vitric tuffs are classified chemically as: 1) high silica rhyolites - $SiO_2 > 72\%$, and 2) subaluminous/peralkaline rhyolites - $Al_2O_3/Na_2O + K_2O + CaO \leq 1$.

In the Sacramento-Majalca area, the late Eocene high silica alkali rhyolitic ignimbrites overlie the older calc-alkalic Peñas Azules volcanics and are overlain by Oligocene rhyolitic ignimbrites. The Peñas

Azules volcanics were probably formed during the Laramide orogeny (late Cretaceous to early Eocene). The late Eocene high silica alkali rhyolites were erupted during Elston's (1976) active stage of extension (late Eocene to Miocene) of the western portion of the American plate. The active stage of extension was followed by the passive stage of extension during the Miocene to present (Elston, 1976). The Oligocene rhyolites of the main Sierra Madre Occidental may have been related to this period of relaxation following compression. The high silica alkali rhyolites near Sacramento are located between the calc-alkalic igneous center of western Mexico and the alkalic igneous center of western Texas. These rocks can be considered intermediate in composition between calc-alkaline and alkaline.

A C K N O W L E D G M E N T S

I would like to thank Ing. Guillermo P. Salas, Director General of Consejo de Recursos Minerales, Mexico, for his assistance and financial support of this investigation. Thanks are also extended to Fernando de la Fuente, also of Consejo de Recursos Minerales, for providing office space in Chihuahua City. Special thanks are extended to the Cano family of Chihuahua City for their gracious hospitality while I was in Mexico during August, 1974, and July, 1975.

I would like to express my appreciation to Dr. Richard L. Mauger who supported this study and guided the laboratory work and final preparation of this thesis. I am grateful to Drs. S. E. Clabaugh and F. W. McDowell of the University of Texas, Austin, and to Dr. B. A. Bishop, East Carolina University, for suggestions and comments made during a visit to the Sacramento area in July, 1975. Dr. Bishop also critically read the thesis. Thanks are extended to Dr. Pei-lin Tien for advice on X-ray diffraction work and for critically reading the thesis. I would also like to thank Dr. Steven Schamel of Lafayette College, Easton Pennsylvania for serving as thesis consultant.

I am greatly indebted to Ruth Gall for assisting me in the Sacramento area during July, 1975, and for typing the final manuscript.

CONTENTS

Page

Abstract iii

Acknowledgments v

Introduction 1

Geographic setting 4

Geologic setting. 5

Stratigraphy 8

Petrology of the ignimbrites. 12
- Nomenclature 12
- Methods of study and sample preparation 13
- Density and porosity. 18
- Jointing. 22
- Petrographic descriptions of the tuff units 31
  - Unit 1. 31
  - Unit 2. 38
  - Unit 3. 45
  - Unit 4. 50
  - Unit 5. 55
- Major elemental analysis 59
  - Data processing. 59
  - Ignimbrite petrochemistry 61
- Cooling units 65
  - Introduction. 65
  - Unit 1. 67
  - Units 2, 3, and 4 70
  - Unit 5. 76

Tectonic implications 78

Conclusions 79

References. 80

TABLES

Table — Page

1. Size terminology classifications 13

Table — Page

2. Mineralogic compositions of ignimbrites determined by X-ray diffraction. 14

3. Composition of sanidine from the ignimbrites determined by X-ray diffraction. 15

4. X-ray diffraction analytical data 16

5. X-ray spectrometer analytical data 17

6. U. S. G. S. granite standard G-2 chemical analysis. . . 18

7. Modal data for the ignimbrite samples 23

8. Average modal data for the ignimbrite units 32

9. Comparison of oxide weight percentages of sample no. 5 determined with and without a correction for matrix absorption 61

10. Oxide weight percentages for the ignimbrites determined by X-ray fluorescence 62

11. Comparison of Na_2O oxide weight percentages for the ignimbrite samples 63

12. Comparison of two determinations of oxide weight percentages of sample no. 9 63

13. Average oxide weight percentages for the ignimbrite units. 64

14. Oxide mole fractions and Al_2O_3/K_2O+Na_2O+CaO mole ratios of the ignimbrite units. 65

ILLUSTRATIONS

Figure — Page

1. Index map of Chihuahua, Mexico 2

2. Geologic map of the area south of Sacramento, Chihuahua, Mexico 3

3. Structure profile of Majalca - Sacramento - Sierra Peña Blanca area. 7

Figure Page

4. Stratigraphic column showing whole rock and rock powder density curves. 9

5. Stratigraphic column showing porosity 10

6. Photograph of Unit 2-A - Unit 2-B contact 11

7. Photograph of Unit 3 - Unit 4 contact 11

8. Photograph of Unit 4 - Unit 5 contact 11

9. Cook's composition triangle for ignimbrites 12

10. Curve for the determination of Or content in sanidine . . 19

11. Stratigraphic column of Unit 1 showing reconstructed porosity curves. 20

12. Stratigraphic column of Unit 2 showing reconstructed porosity curves. 21

13. Idealized sketch of zones of jointing in a Yakima basalt flow 26

14. Stratigraphic column showing jointing patterns for the ignimbrites 27

15. Photograph of Unit 1-A 29

16. Photograph of the base of Unit 1-B 29

17. Photograph of the top of Unit 1-B. 29

18. Photograph of Unit 2-A 30

19. Photograph of the top of Unit 5 31

20. Photomicrograph of Unit 1-A. 33

21. Photomicrograph of Unit 1-A. 33

22. Photomicrograph of Unit 1-A. 36

23. Photomicrograph of Unit 2-A. 39

24. Photomicrograph of Unit 2-A. 39

25. Photomicrograph of Unit 2-A. 42

Figure Page

26. Photomicrograph of Unit 2-B 42

27. Photomicrograph of Unit 2-B 44

28. Photomicrograph of Unit 3 46

29. Photomicrograph of Unit 3 46

30. Photomicrograph of Unit 4 51

31. Photomicrograph of Unit 4 52

32. Photomicrograph of Unit 4 52

33. Photomicrograph of Unit 5 57

34. Diagram illustrating an ash-flow eruption. 66

35. Idealized sketch of an ignimbrite showing welding, porosity, and vitric crystallization trends 68

36. Stratigraphic column showing welding, porosity, and vitric and vapor-phase crystallization. 71

I N T R O D U C T I O N

The town of Sacramento, Chihuahua, Mexico is located approximately 25 km northwest of Chihuahua City on Mexico Highway 45 (Fig. 1). Sacramento lies on the northern flood plain of the Rio Sacramento, 1 km north of the present channel (Fig. 2). Ignimbrites are exposed along the southern edge of the Rio Sacramento flood plain approximately 1 km east of the intersection of Highway 45 and the Rio Sacramento. The outcrop protrudes through a capping of unconsolidated colluvium, alluvial breccias, and gravels.

The purpose of this study is to discern the physical and chemical nature of the volcanic deposits and to attempt to relate them to the regional tectonic and volcanic history.

There has been no detailed geologic work done in the Sacramento area. Mauger (1975) and Gall (1975) briefly described the geology of the Sacramento-Cerro Jesus Maria area and the Sacramento area.

This study is part of the Chihuahua Volcanic Project initiated and directed by Dr. Richard L. Mauger. Field expenses and some laboratory expenses were funded by Consejo de Recursos, Mexico City, Mexico.

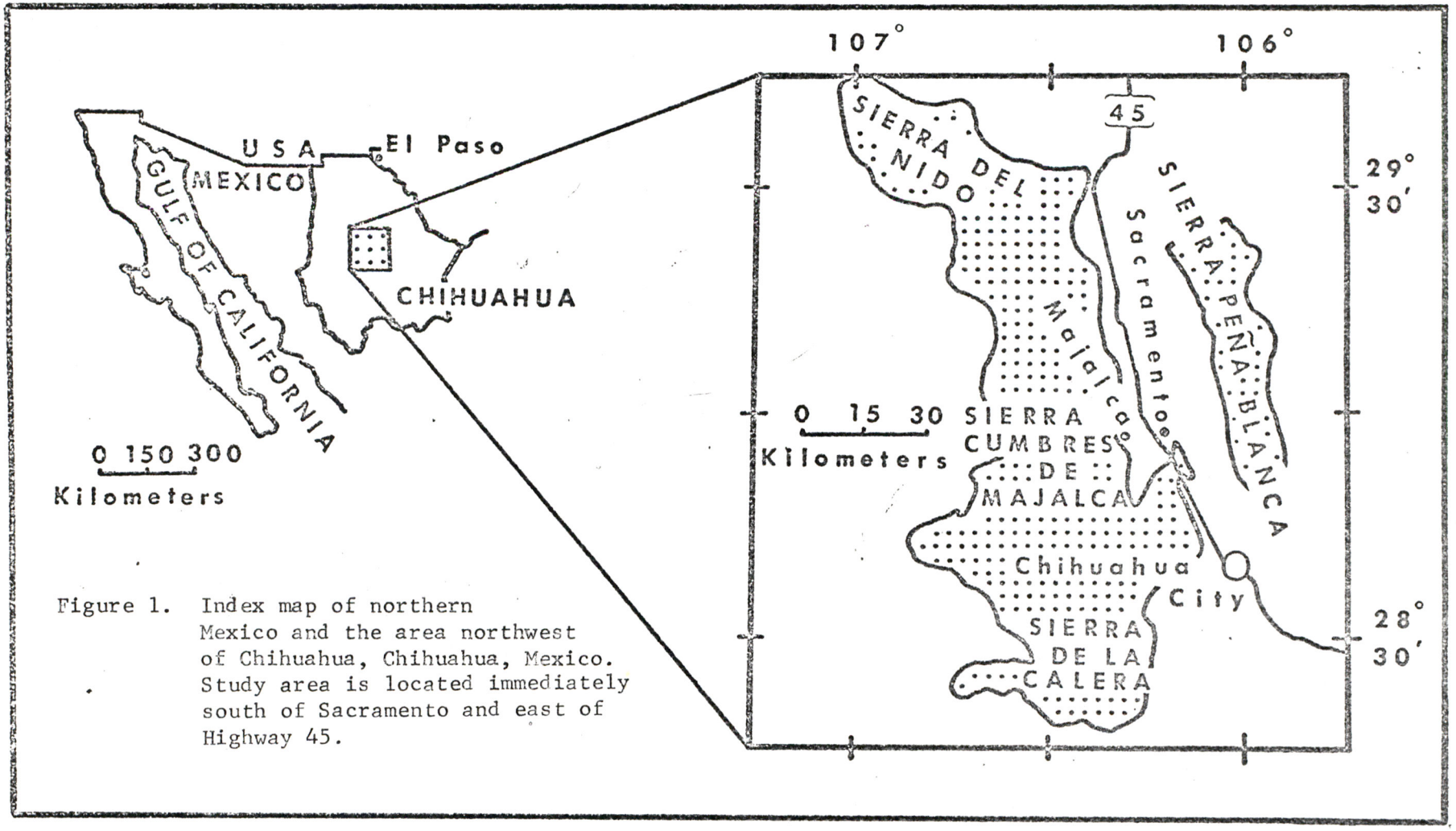

Figure 1. Index map of northern Mexico and the area northwest of Chihuahua, Chihuahua, Mexico. Study area is located immediately south of Sacramento and east of Highway 45.

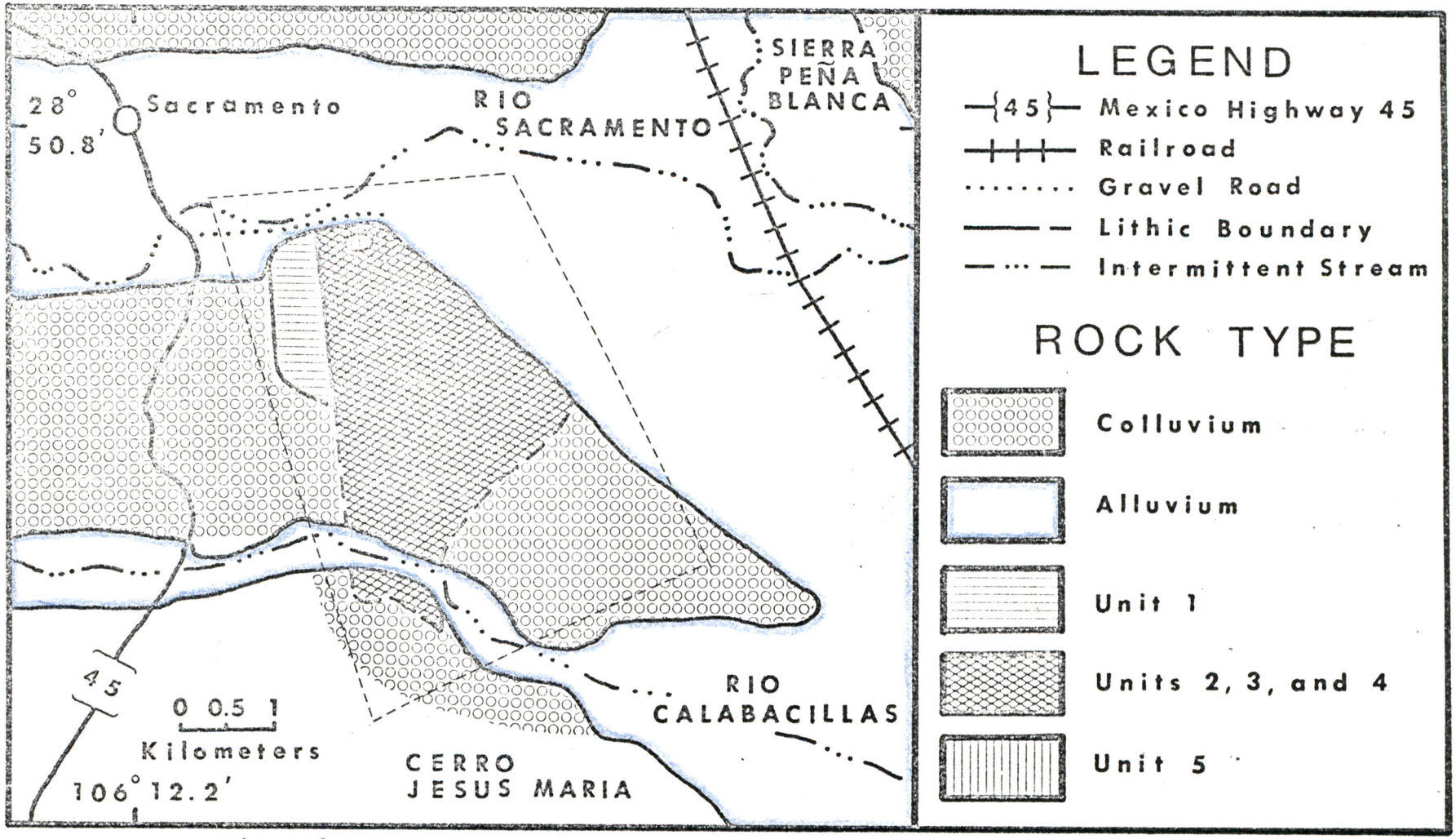

Figure 2. Geologic map of the area south of Sacramento, Chihuahua, Mexico.

G E O G R A P H I C S E T T I N G

The study area is located at long. 106° 12.2' W and lat. 28° 50.8' N and is approximately 1,500 m above sea level. The outcrop area is easily reached via an east-west gravel road that intersects Highway 45 just south of Rio Sacramento (Fig. 2).

The Rio Sacramento begins in the Cumbres de Majalca area and flows to the east side of the Sacramento Valley where it turns to the south and eventually joins the Rio Chuscivar just north of Chihuahua City. The Rio Chuscivar flows east into the Rio Conchos which eventually joins the Rio Grande at Ojinaga, Mexico.

The study area is located in an intermontane basin of the High Basin and Range Province which borders the eastern flank of the Sierra Madre Occidental. The dry shadow effect of the Sierra Madre Occidental produces the semi-arid climate of Chihuahua, Mexico (Schmidt, 1973).

The soils of the Sacramento area belong to the bajada group (Schmidt, 1973) and are found on the alluvial pediments, badlands, older river terraces, and the floors of ancient basins. Generally, these soils have pedogenic horizons, are low in organic matter, and are rarely moist for more than 3 consecutive months. Bajada soils commonly have a clay horizon and/or a gypsum or caliche horizon.

The vegetation of Chihuahua is controlled mainly by elevation, rainfall, and soil type (Schmidt, 1973). The study area is classified as grasslands and oak savanna. The thin soils and seasonal rainfall favor grasses, although oaks find moisture along intermittent streams with ample ground water flow.

G E O L O G I C S E T T I N G

The Chihuahua Trough contained a late Jurassic to Cretaceous sea which was bordered by the Diablo Platform to the northeast, the Aldama Platform to the southwest, and the Coahuila Platform to the southeast (DeFord, 1969). During the Laramide orogeny (late Cretaceous to Eocene), the Cretaceous limestones in the trough were pushed to the northeast against the Diablo Platform. Compressional tectonics relaxed from late Eocene to Miocene and rifting and minor volcanism occurred (McDowell and Keiser, 1976). Extensional tectonics began in the Miocene and were accompanied by fundamentally basaltic volcanism, block faulting, and epeirogenic uplift (Elston, 1976, and McDowell and Keizer, 1976).

The dominant physiographic features of Chihuahua are north-northwest trending mountain ranges with coalescing intermontane basins. The study area is in an intermontane basin between the Cumbres de Majalca to the west and the Sierra Peña Blanca to the east (Fig. 1). The Cumbres de Majalca consists of basaltic and andesitic volcanics and volcaniclastic sediments capped by late Eocene and Oligocene rhyolites (Mauger, 1975, and Spruill, 1976). The Sierra Peña Blanca consist of Cretaceous limestones capped by late Eocene and Oligocene rhyolites (Mauger, 1976, personal communication, and Alba and Chaves, 1974). The intermontane basin is filled with alluvium derived from the surrounding mountain ranges.

The exact relationship between the late Eocene rhyolites of the Sacramento area and those of the Cumbres de Majalca is not yet known. However, Mauger (1975) states that the volcanics of the Sacramento area are high in the late Eocene section and are younger than the rhyolites that are exposed in the Majalca area.

A major fault evidently is located between the Sacramento area and the Sierra Peña Blanca along which the western edge of the Sierra Peña Blanca block is uplifted relative to the eastern margin of the Sacramento block (Fig. 3, Mauger, personel communication). The relationship between the late Eocene rhyolites of the study area and those of the Sierra Peña Blanca is unknown.

The ignimbrites of the Sacramento area strike N 10° W and dip 15° NE and conform to the general low dips of the late Eocene rhyolites farther west (Fig. 3). They are erosionally resistant and form a 0.8 km-long outcrop. Locally cliff faces reach 20 m in height. Some of these rocks are exposed along the southern bank of the Rio Calabacillas (Fig. 2), but locally they are covered by talus from Cerro Jesus Maria. To the north, east, and west of the study area (Fig. 2), the surface consists of alluvium and colluvium which conceal the underlying bedrock.

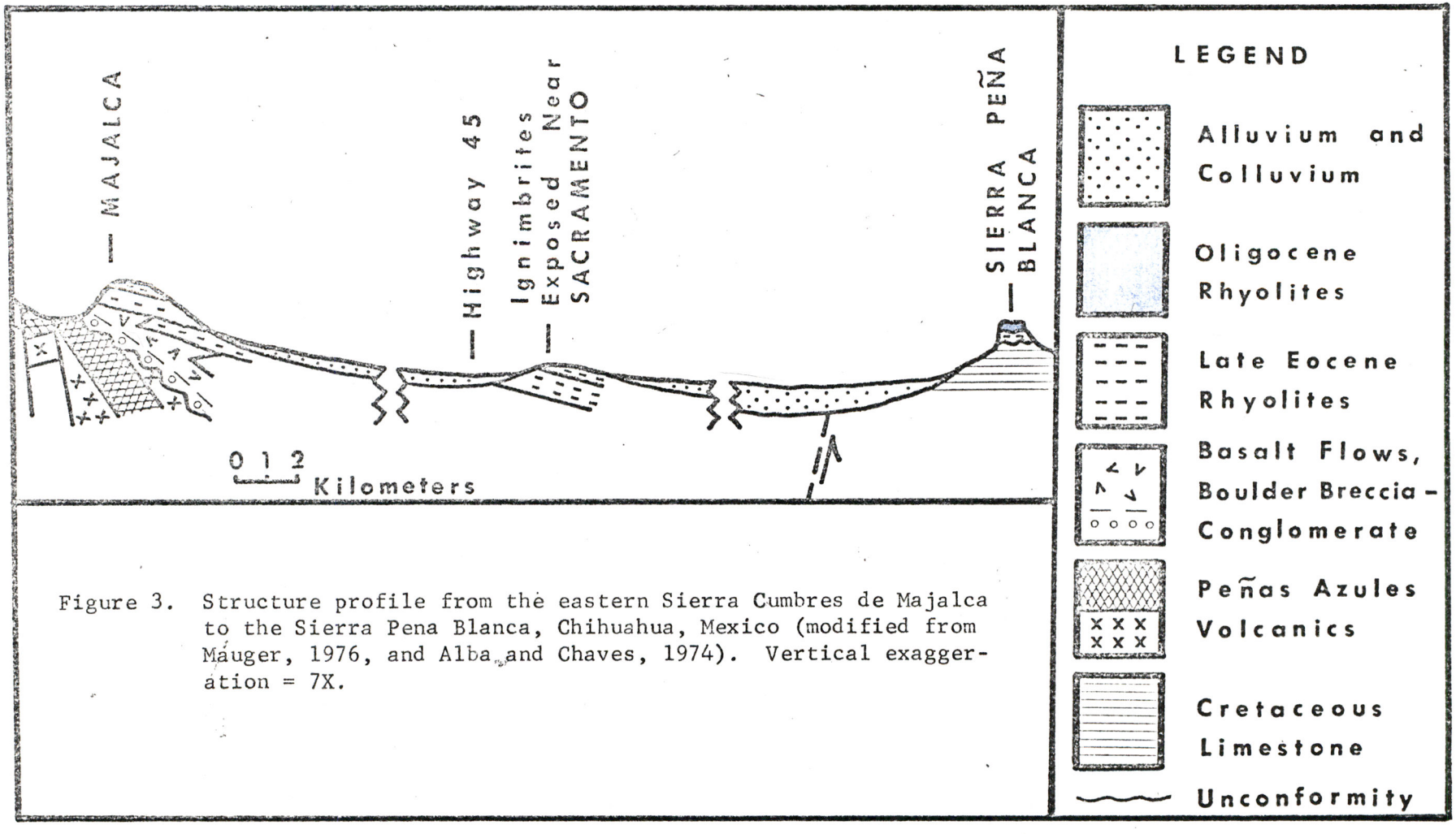

Figure 3. Structure profile from the eastern Sierra Cumbres de Majalca to the Sierra Pena Blanca, Chihuahua, Mexico (modified from Mauger, 1976, and Alba and Chaves, 1974). Vertical exaggeration = 7X.

S T R A T I G R A P H Y

The ignimbrites in the study area are approximately 150 m thick and have an areal outcrop of about four km^2 (Fig. 2). The ignimbrites are five stratigraphic units (Figs. 4 and 5). Unit 1 is a moderately welded crystal-bearing vitric tuff which is about 100 m thick. Unit 1 can be divided into 2 subunits on the basis of the degree of compaction, type of jointing, and porosity. The transition from Unit 1-A (lower 55 m) to Unit 1-B (upper 45 m) takes place over approximately two meters.

Unit 2 is 29 m thick and lies on an erosional surface. Unit 2 can be divided into two subunits on the basis of the degree of compaction, type of jointing, porosity, and color. Unit 2-A (lower 10 m) is an intensely welded vitric tuff (vitrophyre) and Unit 2-B (upper 19 m) is a moderately welded vitric tuff. The transition from Unit 2-A to Unit 2-B takes place over approximately 0.5 m (Fig. 6).

The contact between Unit 2 and Unit 3 is a parting that represents a short break in time between multiple flows of a single cooling unit (Smith, 1960). Unit 3 is a moderately welded crystal-bearing vitric tuff and is 9 m thick.

The contact between Unit 3 and Unit 4 is a parting in which the top of Unit 3 is fused to the bottom of Unit 4 (Fig. 7). Unit 4 is a welded lithic tuff and is 3 m thick.

The contact between Unit 4 and Unit 5 is an erosional surface (Fig. 8). Unit 5 is 7.5 m thick and consists of an altered, unwelded crystal-bearing vitric tuff which grades upward into a moderately welded vitric-lithic tuff. The transition from the unwelded to welded portions of Unit 5 takes place within approximately three meters.

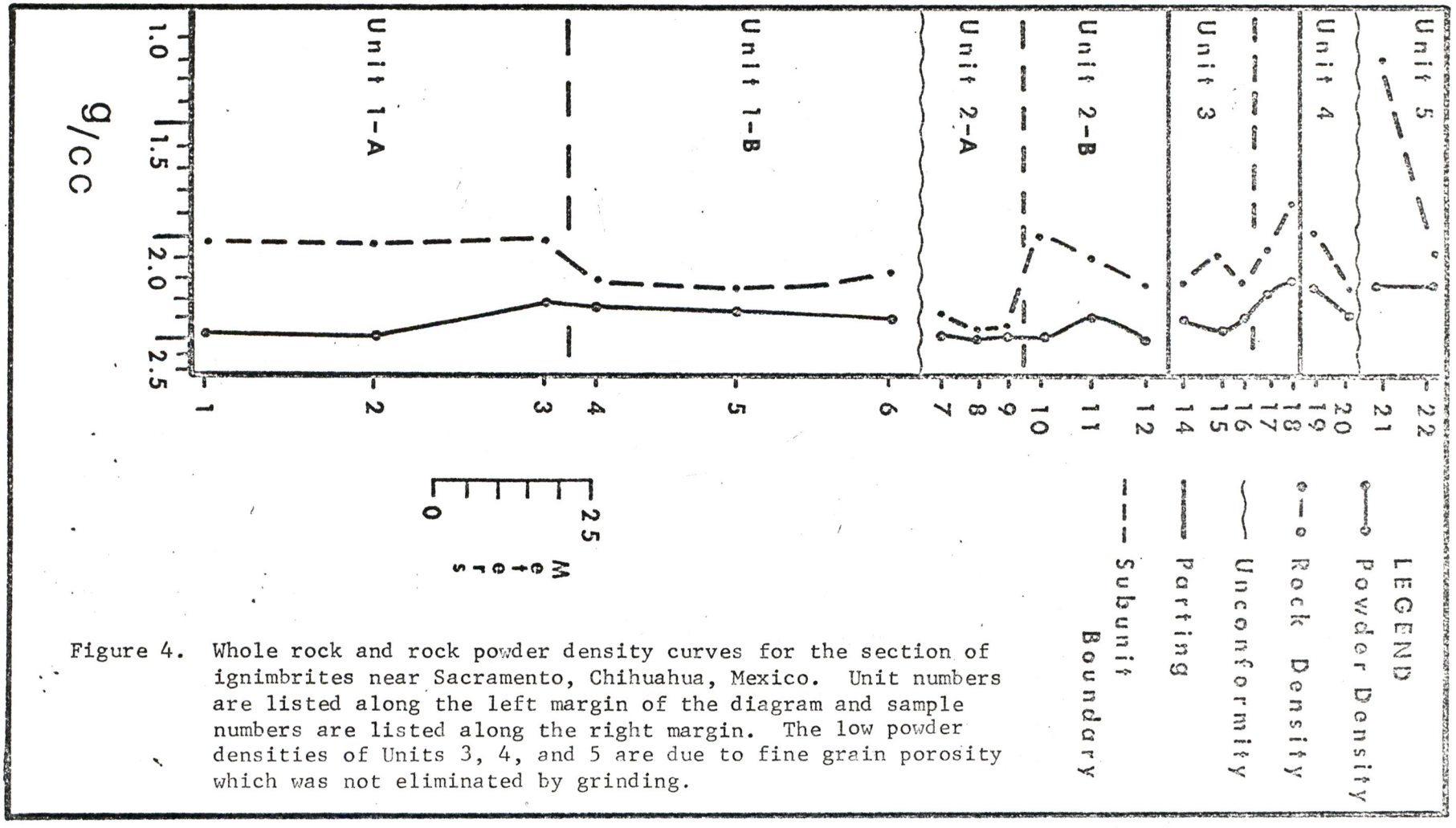

Figure 4. Whole rock and rock powder density curves for the section of ignimbrites near Sacramento, Chihuahua, Mexico. Unit numbers are listed along the left margin of the diagram and sample numbers are listed along the right margin. The low powder densities of Units 3, 4, and 5 are due to fine grain porosity which was not eliminated by grinding.

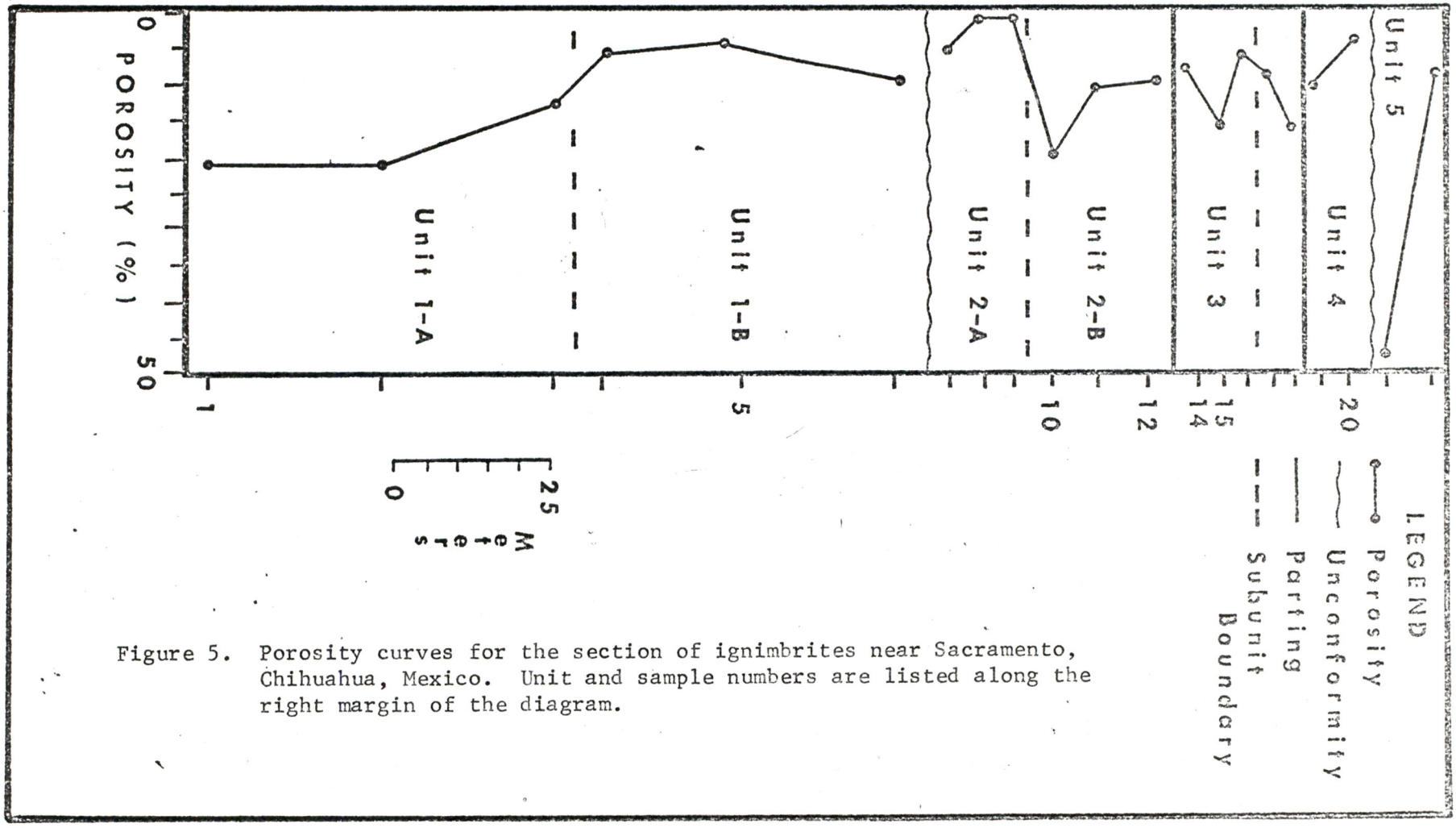

Figure 5. Porosity curves for the section of ignimbrites near Sacramento, Chihuahua, Mexico. Unit and sample numbers are listed along the right margin of the diagram.

Figure 6. Contact between Unit 2-A and Unit 2-B. Photograph of the contact between Unit 2-A (basal vitrophyre) and Unit 2-B showing the transsition (rubbly zone) between the massive basal vitrophyre and the overlying, eutaxitic tuff. The sunglasses (14 cm in length) sit on the 0.5 m thick rubbly zone (Unit 2-A -- Unit 2-B contact).

Figure 7. Contact between Unit 3 and Unit 4. Photograph of the contact (a) between Unit 3 (crystal-bearing vitric tuff) and Unit 4 (lithic tuff). The top of Unit 3 is fused to the bottom of Unit 4. The dark gray, disc-shaped areas are lithic fragments (b). The small black areas are cavities (c). The white areas are botryoidal quartz (d) that filled cavities. The black marker is 10 cm in height.

Figure 8. Contact between Unit 4 and Unit 5. Photograph of the contact (c) between Unit 4 (lithic tuff) and Unit 5 (vitric-lithic tuff). The contact is an erosional surface. The units dip about 15 to the east (left). Resistant vertical face in lower left about 1.5 m high. Note the recessive nature of the basal portion of Unit 5.

PETROLOGY OF THE IGNIMBRITES

NOMENCLATURE

Cook (1965) and Macdonald (1972) proposed that the term ignimbrite be used strictly as a rock unit term, freed from welding, size-range, and compositional restrictions. According to this usage, ignimbrites are equivalent to the ash-flow cooling units of Smith (1960) and to the ash-flow tuffs of Ross and Smith (1961). Welded tuff and unwelded tuff are used as rock-type terms.

The determination of rock types is based upon Cook's (1965) composition triangle for ignimbrites (Fig. 9). Grain size nomenclature

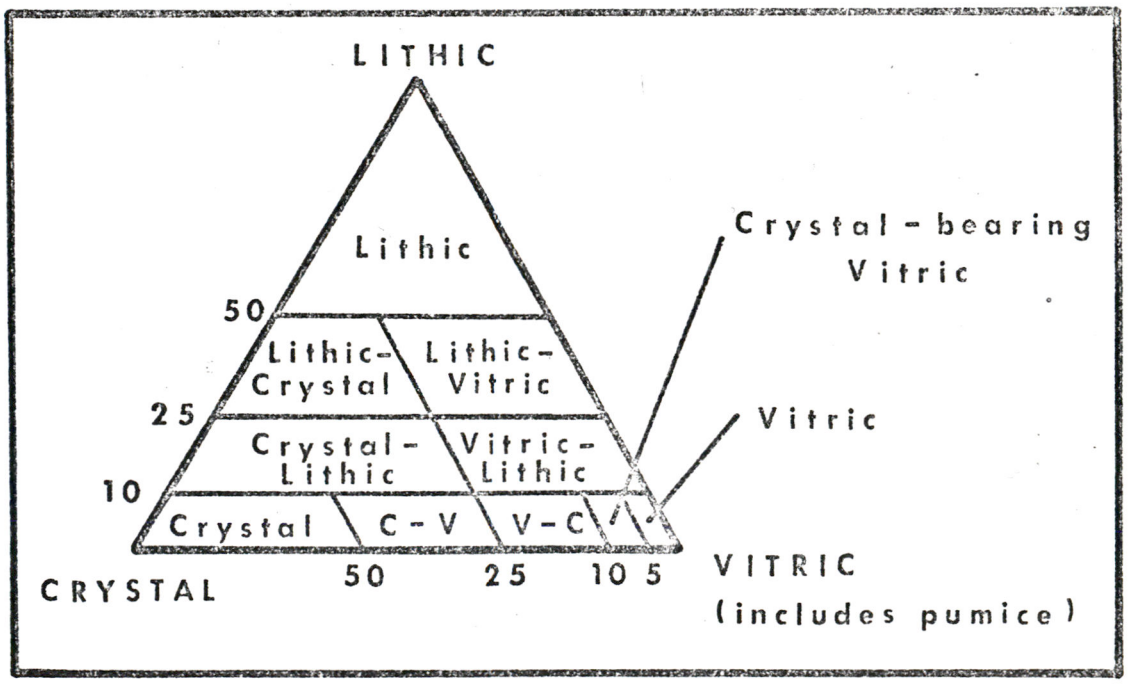

Figure 9. Compositional triangle for ignimbrites (modified from Cook, 1965). The C-V means crystal-vitric and V-C means vitric-crystal.

is taken from Wentworth's classification for clastic fragments (modified by Folk, 1974), and from Fisher's classification (1960) for volcanic fragments (Table 1). The rock color chart of Goddard and others (1963) is used as the reference for rock colors.

SIZE (mm)	Wentworth	Fisher
256 - 64	Cobble	Fine Block
64 - 4	Pebble	Lapilli
4 - 2	Granule	
2 - 0.5	Coarse Sand	Ash
0.5 - 0.25	Medium Sand	
0.25 - 0.0625	Fine Sand	coarse
0.0625 - 0.0039	Silt	0.0625 fine
0.0039 and less	Clay	

Table 1. A comparison of Wentworth's terms for the classification of fragment sizes (modified by Folk, 1974) with Fisher's (1960) terms.

METHODS OF STUDY AND SAMPLE PREPARATION

The volcanic section near Sacramento was measured, described, and sampled (Fig. 4) during August, 1974, and July, 1975.

A petrographic microscope and point counter were used to study petrographic thin sections. The mineral composition of the aphanitic rocks (Table 2) and the Na/K ratio in sanidines (Table 3) were determined by X-ray diffraction methods (Tables 4a and 4b).

	SANIDINE	QUARTZ	CRISTO-BALITE	TRIDYMITE	SMECTITE GROUP CLAY	UNIT
22	major	major	major	minor	absent	5
21	minor	absent	absent	absent	major	
SAMPLE 19-20	major	minor	major	minor	absent	4
SAMPLE 14-18	major	minor	major	minor	absent	3
SAMPLE 11-12	major	minor	major	major	absent	
SAMPLE 10	major	major	minor	absent	absent	2
SAMPLE 7-9	major	minor	major	absent	absent	
1-6	major	major	minor	minor	absent	1

Table 2. X-ray diffraction analyses for major and minor minerals in ignimbrites near Sacramento, Chihuahua, Mexico. Relative proportions of minerals estimated by intensity of prominent reflections.

The major elemental analyses were done by using an X-ray spectrometer (Table 5). This method provides rapid, nondestructive qualitative and quantitative chemical analysis by measuring the characteristic secondary radiation emitted from a sample pellet which is excited by bombardment with high energy X-rays (Allman and Lawrence, 1972). A fixed counting time of 25 seconds was used. The method for establishing the correct fixed counting time has been discussed by Mack and Spielberg (1958). Three 25 second counting intervals give a precision of $\pm$1% with a 90% confidence level for the peak intensities. Peak intensities of an unknown were compared to those of U. S. G. S. granite standard G-2 (Table 6). Use of the comparison method also affords a constant check on machine drift and operator error (Allman and Lawrence, 1972). A die and hydraulic press were used to make pellets 3.3 cm in diameter, 3 mm in thickness, and 3.3 g in weight. Each powdered sample was pressed to

		HOMOGENIZED ROCK SAMPLE	HOMOGENIZED SANIDINE SEPARATE	UNIT
	22b	Or_{49}	Or_{39}	5
	22a	Or_{53}		
	20	Or_{49}		4
	19	Or_{47}		
	18	Or_{49}		
	17	Or_{47}		
S	16	Or_{47}		3
A	15	Or_{47}		
M	14	Or_{49}		
P				
L	12	Or_{45}		
E	11	Or_{48}		
	10	Or_{47}		2
	9	Or_{49}		
	8	Or_{49}		
	7	Or_{50}		
	6	Or_{50}	Or_{49}	
	5	Or_{48}	Or_{47}	
	4	Or_{48}	Or_{69}	1
	3	Or_{48}	Or_{47}	
	2	Or_{47}	Or_{42}	
	1	Or_{49}	Or_{62}	

Table 3. Composition of sanidines from the ignimbrites near Sacramento, Chihuahua, Mexico. Assumes 10% An in sanidine.

2,109 kg/cm^2 (30,000 lb/in^2) and left in the press until the pressure stabilized around 1,758 kg/cm^2 (25,000 lb/in^2). The pellets were removed from the press, wrapped in parafilm, and stored in a desiccator before the analyses.

Whole rock samples and phenocryst separates were ground for 20 minutes using a McCrone micronizing mill and corundum grinding elements to produce uniform clay-size, well mixed powders. The grinding reduces all particles to less than 60 μm in diameter. Rock powders (3.0 g) and

MINERAL	2θ	dÅ	hkl	I/I_o
Quartz	20.9	4.3	100	35
	26.7	3.3	101	100
Cristo-balite	21.9	4.1	101	100
	36.1	2.5	200	20
Tridymite	20.8	4.3	200	100
	21.8	4.1	002	90
	23.4	3.8	201	90
	30.2	3.0	$20\bar{2}$	60
Sanidine	23.7	3.8	130	75
	27.3	3.3	220	75
	27.4	3.3	202	100
	27.7	3.2	002	90

Table 4a. Prominent diffraction peaks of minerals from the ignimbrites near Sacramento, Chihuahua, Mexico. I/I_o is the ratio relative to the peak with highest intensity (ASTM Cards).

AMPL. GAIN	E_l	E_u	H.V.	RADIATION
16	220	360	140	Cu

Table 4b. Pulse height settings, amplifier gain, and high voltage setting for GE model XRD-6 X-ray diffractometer utilizing copper radiation.

methyl cellulose (0.3 g) were ground together as an ethanol slurry. This insures complete mixing and minimum wear of grinding elements. The methyl cellulose serves as a binding agent and is necessary to make mechanically strong pellets. Methyl cellulose is composed of light elements that do not give characteristic lines in the spectrometer. Experiments show that Al_2O_3 contamination of samples milled with corundum grinding elements is insignificant. The U. S. G. S. rock standards were also not corrected for Al_2O_3 added by grinding (Flanagan, 1967).

	Al	Si	K	Ca	Ti	Fe
Atomic Number	13	14	19	20	22	26
Target	Cr	Cr	Cr	Cr	Cr	W
Crystal	PET	PET	LiF	LiF	LiF	LiF
X-ray Path	vac.	vac.	vac.	vac.	vac.	air
Ampl. Gain	1	1	1	1	1	16
H.V.	175	172	168	167	165	136
Milli-amps	10	10	6	6	10	10
K.V.	45	45	45	45	45	45
Plates	brass	brass	Al	Al	Al	Al
Back-ground	136.65	105.70	129.85	107.25	82.35	54.65
2 θ		113.70	144.85	116.25	91.35	60.65
Peak 2 θ	144.65	108.70	136.85	113.25	86.35	57.65
E_L	150	100	50	90	105	95
E_U	360	340	325	300	290	250

Table 5. Instrumental settings for GE model SPG-5 X-ray spectrometer analyses of Al, Si, K, Ca, Ti, and Fe. A flow proportional counter was used for all determinations.

OXIDE	WEIGHT PERCENT
Al_2O_3	15.42
SiO_2	69.21
K_2O	4.45
CaO	1.96
TiO_2	0.47
Fe_2O_3	2.66

Table 6. Weight percentages of Al_2O_3, SiO_2, K_2O, CaO, TiO_2, and Fe_2O_3 in U.S.G.S. granite standard G-2 according to Hutchison (1974).

Phenocrysts were separated with limited success by leaching rock samples with HF.

The original sanidines (phenocrysts and groundmass) are cryptoperthites. They were homogenized at a temperature of 900° C for 3 to 4 hours following the method given by Tuttle and Bowen (1958). At temperatures greater than 900° C there is complete solid solution between Na- and K-feldspar (Bowen and Tuttle, 1950). The 2θ position of the $\bar{2}01$ peak for homogenized sanidine ranges from 22° for pure Na-feldspar to 21° for pure K-feldspar (Fig. 10). The $\bar{2}01$ sanidine peak is measured relative to the 100 peak ($2\theta = 20.85°$) of quartz (supplied by Fisher Scientific Co.). The d-value of the 100 peak of the quartz standard was checked relative to the d-value of the 101 peak of $KBrO_3$ (Orville, 1967).

DENSITY AND POROSITY

The density of rock powders was measured by weighing a powder sample in air and then using the immersion method to obtain volume.

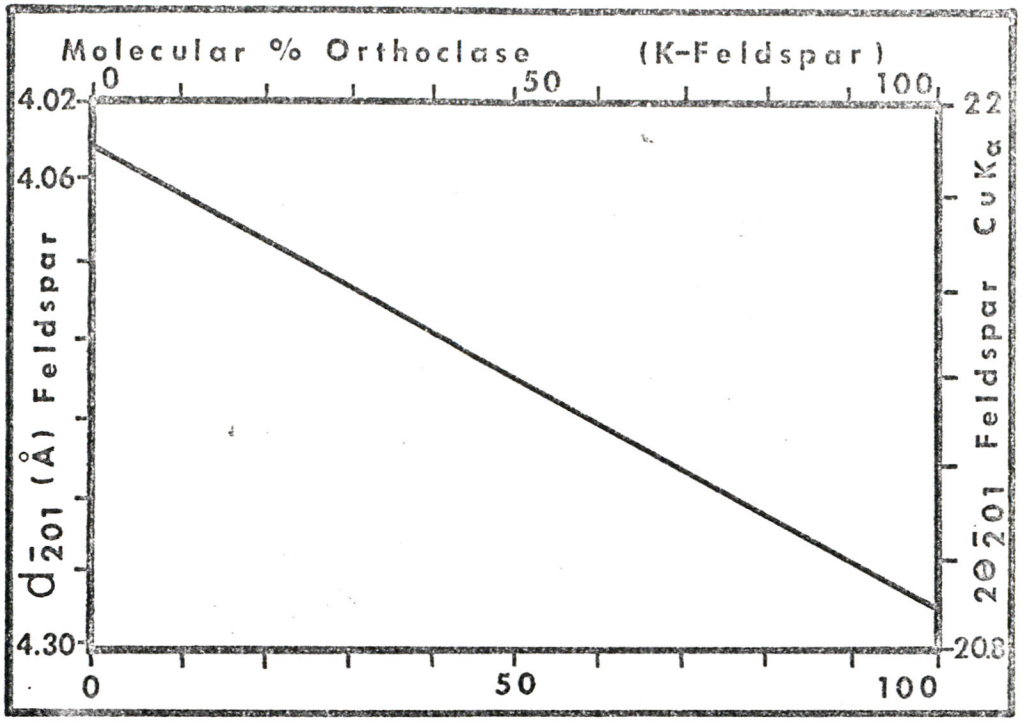

Figure 10. Curve for determining the Or content of sanidine by X-ray diffraction (from Orville, 1963, and Jones and others, 1969). Assumes 10% An in sanidine.

Rock densities were measured by cutting a rectangular block of each sample. The volumes were measured directly and the blocks were weighed in air (Fig. 4). The difference between the powder density and the rock density divided by the powder density gives porosity (Fig. 5).

The porosity varies with the degree of compaction, with the degree of vapor-phase crystallization, and with the extent of ground water deposition in pore space. Intensely welded portions of ignimbrites undergo high degrees of compaction while unwelded portions usually undergo less; therefore the porosity tends to vary inversely with welding and compaction. A decrease in compaction is accompanied by an increase in pore space for vapor-phase crystallization which can significantly reduce porosity by mineral infilling. The deposition of botryoidal

quartz in pore space from percolating ground water can also reduce porosity.

Unit 1 comprises the lower middle to upper middle portion of a relatively thick ash flow (Fig. 11). The ignimbrite is composed primarily of sanidine and SiO_2 polymorphs (Table 2) and has a powder density of 2.4 g/cc (Fig. 4). Unit 1-A represents the lower middle portion of the ignimbrite. The shards are moderately welded and compacted, but the pumice lumps did not collapse completely (19% porosity). Unit 1-B represents the upper middle portion where compaction was more intense, as indicated by more collapsed pumice lumps (7% porosity).

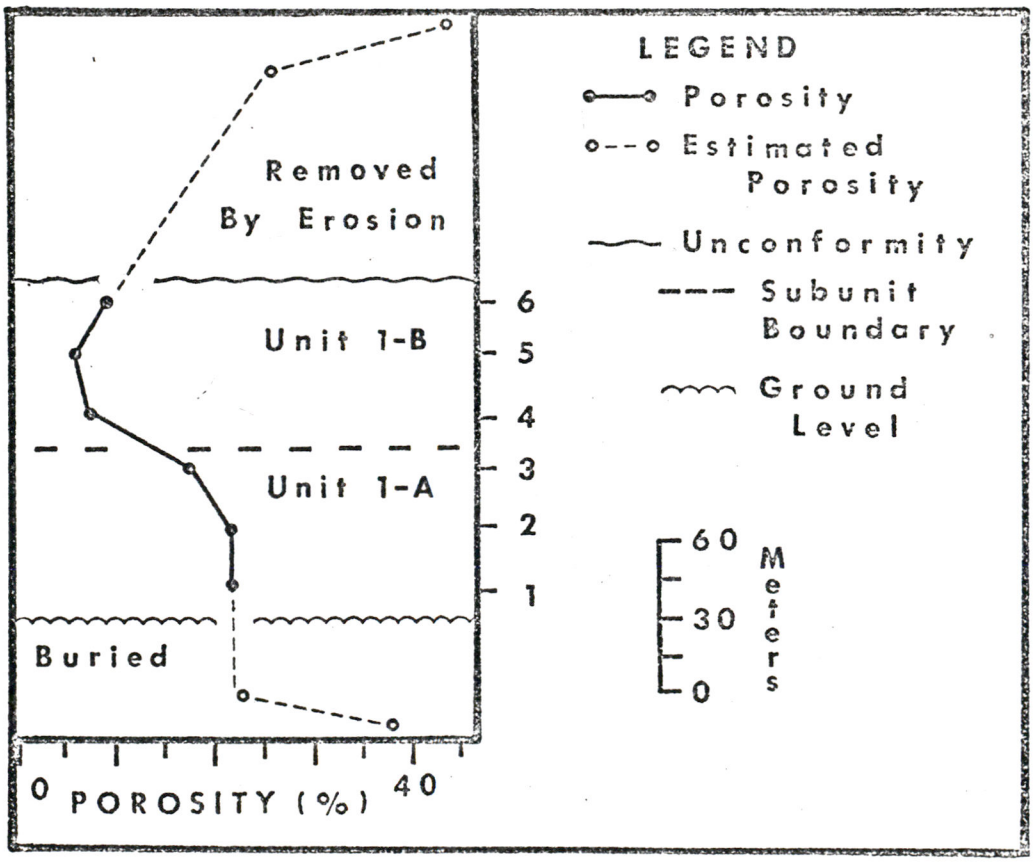

Figure 11. Measured and reconstructed porosity curves for Unit 1, Sacramento, Chihuahua, Mexico. Sample numbers are listed to the right of the diagram.

Unit 2 is composed of sanidine and SiO_2 polymorphs (Table 2), and has a powder density of 2.5 g/cc (Fig. 4). Unit 2-A is a basal vitrophyre with the lowest measured porosity (1.4%) and the highest rock density (2.5 g/cc). Unit 2-B is a moderately welded and compacted tuff with flattened pumice lumps (13.4% porosity). In Unit 2-B, porosity decreases upward in the section and this is opposite that expected for a single-flow cooling unit (Ross and Smith, 1961). The explanation for the anomalous trend is that Units 2, 3, and 4 are a multiple-flow, single cooling unit. Figure 12 is a reconstruction of the porosity curve of Unit 2 prior to the emplacement of Units 3 and 4. The unconsolidated

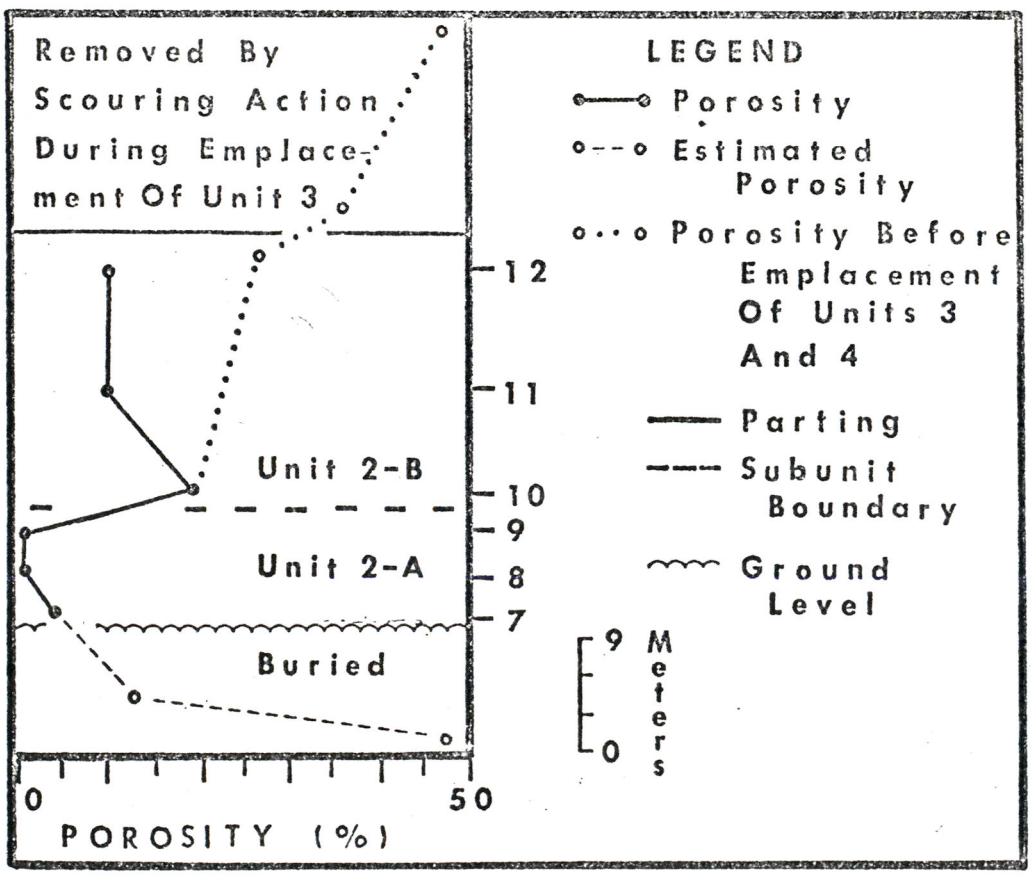

Figure 12. Measured and reconstructed porosity curves for Unit 2, Sacramento, Chihuahua, Mexico. Sample numbers are listed to the right of the diagram.

top of Unit 2 was removed prior to the deposition of Units 3 and 4. The additional overburden due to Units 3 and 4 caused a further reduction in the porosity of Unit 2.

Unit 3 is composed of sanidine and SiO_2 polymorphs (Table 2), and has a powder density of 2.4 g/cc (Fig. 4). The porosity trend for sample nos. 14, 15, and 16 (Fig. 5) is similar to that of Unit 2 B where an upward decrease in porosity is due to additional overburden being added prior to complete lithification of the unit. The increasing porosity trend for sample nos. 17 and 18 (Fig. 5) is probably due to an increase in the content of lithic fragments (Table 7). This change is responsible for the decrease in compactability.

Unit 4 is composed of sanidine and SiO_2 polymorphs (Table 2), and has a powder density of 2.35 g/cc (Fig. 4). The lower portion of Unit 4 is less compacted than the upper portion (Fig. 5) which is truncated by an erosional surface on which Unit 5 was deposited. Unit 4 probably represents the lower half of the upper ignimbrite of the multiple-flow, single cooling unit.

Unit 5 is composed of sanidine and SiO_2 polymorphs (Table 2), and has a powder density of 2.25 g/cc (Fig. 4). The lowermost portion of this unit is a highly altered unwelded tuff (50% porosity and 1.14 g/cc density) which grades upward into a moderately welded tuff (8% porosity and 2.1 g/cc).

JOINTING

Columnar and horizontal joints commonly develop in welded tuffs due to contraction upon cooling and perhaps due to stress corosion

	Sample Nos.	1	2	3	4	5	6	7	8	9	10	11
	Shards	61.3	53.5	56.4	55.1	63.6	61.7	81.7	91.2	91.6	77.0	89.1
	Pumice	31.2	37.5	33.0	37.5	27.9	32.0	18.2	8.3	6.0	22.9	9.6
	Sanidine	5.9	7.6	8.0	4.3	6.0	4.2	0.1	0.3	0.3	0.3	0.8
	Quartz	1.5	1.1	1.0	1.7	0.8	0.5					
T_1	Plagioclase		0.1	1.2	1.0	1.3	1.4				0.1	
	Magnetite		0.2	0.3	0.1	0.2	0.1					0.4
	Hornblende		0.2	0.1	0.1	0.1	0.2					
	Sphene			0.1	0.1	0.1						
	Lithics								0.1	2.1		0.1
	Vitric	92.5	90.9	89.5	92.6	91.5	93.7	99.9	99.8	99.7	99.8	98.8
T_2												
	Phenocrysts	7.5	9.1	10.5	7.4	8.5	6.3	0.1	0.3	0.3	0.3	1.2

T_1 - Modal data in volume percentages.

T_2 - Modal data recalculated to exclude lithics.

* - Ash-size component comprised of lithic fragments.

n/a- Groundmass not vitric.

12	14	15	16	17	18a	18b	19	20	22	
88.2	60.6	55.4	63.9	62.9	60.7	62.7	50.0*	52.4*	70.6	Shards
9.9	30.2	35.7	25.9	28.1	32.0	30.3	20.0	20.8	15.2	Pumice
1.5	7.7	5.5	4.4	3.5	3.5	2.2	5.8	8.8	2.4	Sanidine
										Quartz
										Plagioclase
0.4	0.2	0.6	0.5	0.1	0.1	0.3	0.1			Magnetite
	0.1			0.2	0.1			0.2		Hornblende
										Sphene
	1.3	2.9	5.3	5.2	3.7	4.5	24.0	17.9	11.9	Lithics
98.1	92.0	93.8	94.9	96.0	96.1	97.4	n/a	n/a	85.8	Vitric
1.9	8.0	6.2	5.2	4.0	3.9	2.6	n/a	n/a	2.4	Phenocrysts

Table 7. Modal data, in volume percentages, for the ignimbrites near Sacramento, Chihuahua, Mexico.

cracking. According to Ross and Smith (1961), jointing characteristics are controlled by such factors as rate of cooling, thickness, and degree of welding.

Unit 1 conforms to Swanson's (1967) model for jointing patterns in basalt flows (Fig. 13). Unit 1-A is in the lower middle portion of the deposit (Fig. 4) and is the colonnade (Fig. 14). It consists of 2 m wide, poorly developed columnar and blocky joints (Fig. 15) and is separated from Unit 1-B by a relatively sharp contact. Unit 1-B is in the upper middle portion of the deposit (Fig. 4) and constitutes the entablature (Fig. 14). It consists of 1.5 m wide, well developed columnar and blocky joints at its base (Fig. 16) which are split upwards by a steadily increasing number of dividing joints and blocky joints. The columns at the top of Unit 1-B measure 20 cm in width and horizontal joints are 30 cm in height, causing the rock to break out in equant blocks (Fig. 17). The upper portion of Unit 1-B developed some fanning columnar structure (Fig. 14). The joint surfaces of Unit 1-B are changed in color from grayish orange-pink (5YR 7/2) to light gray (N7) and are the sites of vapor-phase crystallization.

Columnar jointing is poorly developed, but horizontal jointing is well developed in Unit 2-A (Fig. 18). The jointing pattern is similar to the platy joint zone of the colonnade (Fig. 13). The horizontal joints are spaced 10 cm apart while the columnar joints are spaced 30 cm apart. The columnar joint spacing of Unit 2-B is from 30 to 60 cm and the columns are well developed. The columns are split by poorly developed dividing joints and are broken by blocky joints (Fig. 14).

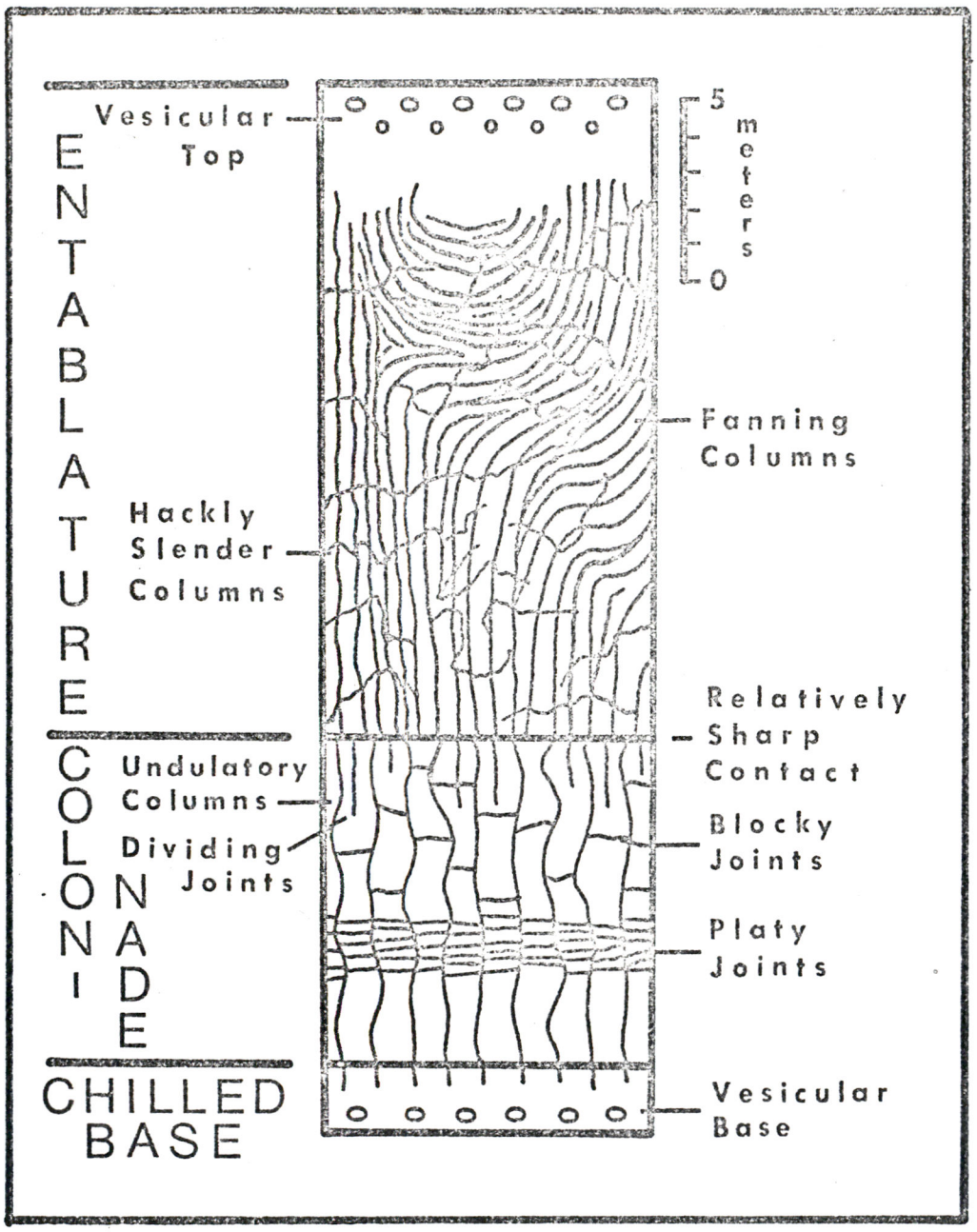

Figure 13. Idealized sketch of zones of jointing in a Yakima basalt flow (from Swanson, 1967).

Figure 14. Jointing patterns in the ignimbrites near Sacramento, Chihuahua, Mexico. Unit 1-A is split by 2 m wide, poorly developed, undulatory columnar and blocky joints. Unit 1-B is split by 1.5 m wide, well developed columnar and blocky joints at its base which are split upwards by a steadily increasing number of dividing and blocky joints. Some fanning columnar structures are developed in the top of Unit 1-B. The transition from Unit 1-A to Unit 1-B takes place over approximately two meters. The joint surfaces of Unit 1-B are altered from grayish orange-pink (5YR 7/2) to light gray (N7) and are the sites of vapor-phase crystallization. Unit 2-A has poorly developed columnar jointing (30 to 60 cm spacing) and well developed platy jointing (15 cm joint spacing). Well developed columnar joints in Unit 2-B are spaced 30 to 60 cm apart and the columns are split by poorly developed blocky and dividing joints. Poorly developed columnar joint spacing, in Unit 3, ranges from 1 to 1.5 m, and the columns are split by blocky joints. In Unit 4, poorly developed columnar and blocky jointing is spaced about 2 m apart. The joints of Unit 4 are sites of botryoidal quartz precipitation. Columnar and blocky joint spacing is from 10 to 30 cm in Unit 5, and the joint surfaces are sites of vapor-phase crystallization.

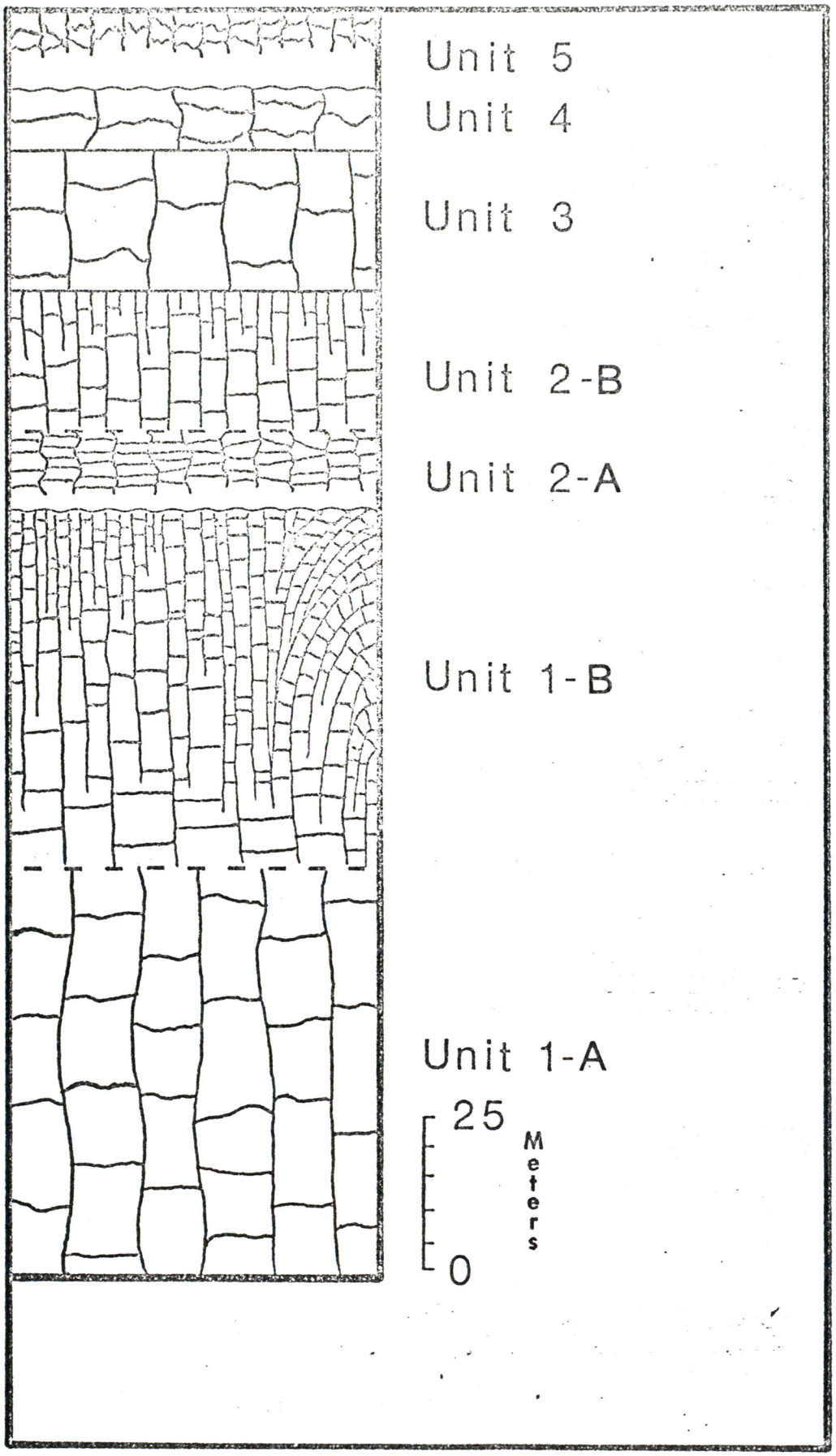

Figure 14

Figure 15. Unit 1-A. Photograph of Unit 1-A (moderately welded, crystal-bearing vitric tuff) showing poorly developed, undulatory columnar and blocky joints. The disc-shaped cavities are relict pumice lumps. The rock hammer in left center of photograph gives the scale.

Figure 16. Unit 1-B. Photograph of the base of Unit 1-B (moderately welded, crystal-bearing vitric tuff) showing well developed columnar and blocky joints.

Figure 17. Unit 1-B. Photograph of the top of Unit 1-B (moderately welded, crystal-bearing vitric tuff) showing columnar, blocky, and dividing joints. Note changes in jointing from Unit 1-A (Fig. 15) to base of Unit 1-B (Fig. 16) and to top of Unit 1-B.

Figure 18. Unit 2-A. Photograph of intensely welded vitric tuff (basal vitrophyre) near Sacramento, Chihuahua, Mexico. Platey and columnar joints were developed and dip is 10° to the east. Note rock hammer in right center of photograph for scale.

Columnar joint spacing in Unit 3 is from 1 to 1.5 m. The columns are poorly developed and are broken by blocky joints (Fig. 14).

Columnar and horizontal jointing was developed in Unit 4 (Fig. 14), so blocks about 2 m in width and thickness typically break out from the cliff wall. Open space along joints are the sites of botryoidal quartz precipitation. A one meter-thick vertical pitchstone dike with vertical foliation was observed to cut across Unit 4.

In the welded portions of Unit 5, small-scale columnar and blocky jointing was developed (Fig. 19). Thus, the outcrop breaks into equant blocks from 10 to 30 cm in length. The joint surfaces are the sites of vapor-phase crystallization.

Figure 19. Unit 5. Photograph of moderately welded vitric-lithic tuff. Columnar and blocky joints were developed.

PETROGRAPHIC DESCRIPTIONS OF THE IGNIMBRITES

Unit 1

The ignimbrite of Unit 1 consists of 59% devitrified groundmass, 33% devitrified pumice lumps, and 8% phenocrysts (Table 8a), and is a welded crystal-bearing vitric tuff (Fig. 9). The relict shards are grayish orange-pink (5YR 7/2) and the relict pumice sites are light gray (N7). The colors are consistent throughout the unit.

The relict shard structure is well preserved in Unit 1-A (Fig. 20) and poorly preserved in Unit 1-B. The glassy material deformed easily, especially around rigid objects like phenocrysts and lithic fragments, and to a lesser extent, around pumice lumps. Deformed shards range from fine to medium sand-size. Relict shard outlines are conspicuous in Unit 1-A, but the high degree of compaction has distorted the primary

	Unit	1-A	1-B	1	2-A	2-B	2	3	4	5
ROCK COMPONENT	Shards	57.1	60.1	58.6	88.9	84.8	86.8	63.6	57.2*	70.6
	Pumice	33.9	32.5	33.2	10.9	14.2	12.5	31.4	20.4	15.2
	Phenocrysts	9.0	7.4	8.2	0.2	1.2	0.7	5.0	7.5	2.4
	Lithics								21.0	11.9

* - Ash-size component consists of lithic fragments.

Table 8a. Average modal data for the ignimbrites near Sacramento, Chihuahua, Mexico. Rock components in volume percentages.

	Unit	1-A	1-B	1	2-A	2-B	2	3	4	5
PHENOCRYSTS	Sanidine	79.7	65.1	72.4	100	77.4	88.7	93.4	98.2	100
	Quartz	13.8	13.7	13.8						
	Plagioclase	4.0	17.1	10.6						
	Magnetite	1.0	1.6	1.3		22.6	11.3	5.1	0.6	
	Hornblende and/or Biotite	0.7	1.8	1.3				1.5	1.2	
	Sphene	0.7	0.8	0.8						

Table 8b. Average modal data for the ignimbrites near Sacramento, Chihuahua, Mexico showing phenocryst volume percentages.

shape of the shard. The deformed shards occur as curved plates, wedges, and Y's. The deformed shard structures in Unit 1-B are mostly obliterated but the few visible outlines are similar to those of Unit 1-A. The glassy portion of Unit 1 crystallized to spherulitic and axiolitic intergrowths (Fig. 21) of sanidine and SiO_2 polymorphs (Table 2). The

Figure 20. Unit 1-A. Color photomicrograph (plane polarized light) of moderately welded, crystal-bearing vitric tuff. Relict shard structures are visible in the center of the photograph. Axiolitic structures within relict shards are faintly visible. In hand specimen, areas of relict shards are grayish orange-pink (5YR 7/2) and relict pumice lumps are light gray (N7). All phenocrysts in the photograph are sanidine.

Figure 21. Unit 1-A. Color photomicrograph (crossed nicols) of moderately welded, crystal-bearing vitric tuff. The spherulitic areas of sanidine and cristobalite coincide with areas of relict shards. The relict pumice lumps underwent granophyric crystallization to sanidine and quartz. They are the light, coarser grained areas between the spherulites. In hand specimen, areas of spherulites (relict shards) are grayish orange-pink (5YR 7/2) and relict pumice is light gray (N7).

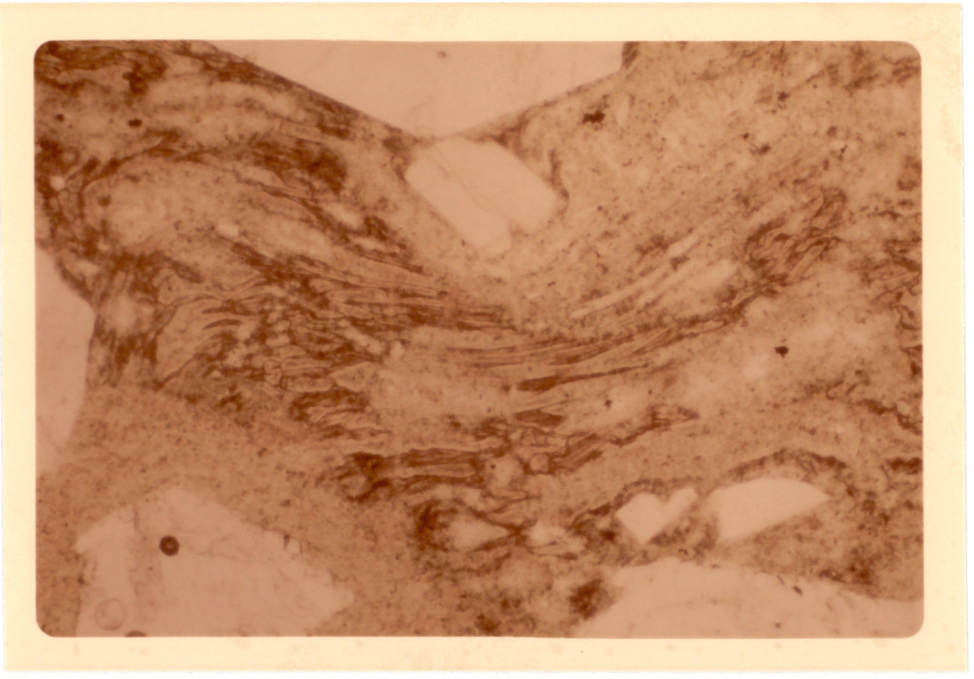

Figure 20

0 0.5
mm

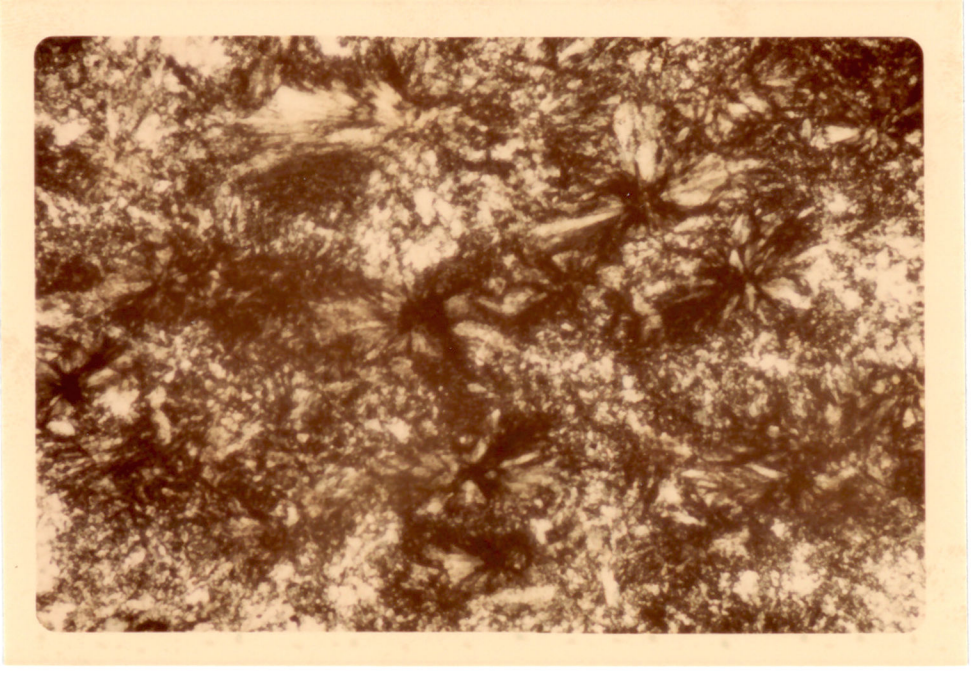

Figure 21

0 0.25
mm

glassy fraction of Unit 1-B crystallized to a massive, clay-size mosaic of equidimensional sanidine and SiO_2 polymorph grains.

The flattened pumice of Unit 1 is typical of eutaxitic texture (Smith, 1960). Pumice shape is more irregular for the larger lumps and the degree of flattening varies, but most pumice lumps are disc-shaped with the plane of flattening parallel to the bedding plane. Toward the top of Unit 1, the pumice lumps decrease in maximum diameter from 7 cm to 1 cm and in maximum height from 2 cm to 3 mm, but the percentage of pumice remains constant (33%). The contact between the pumice and matrix is sharp. The pumice lumps commonly contain any of the phenocrysts found in Unit 1. The pumice is crystallized to a silt-sized mosaic of equidimensional sanidine and quartz grains. The grain size increases inward from the edge of the pumice lump (Fig. 22). The pumice lumps commonly have central cavities which are lined with vapor-phase tridymite and sanidine crystals. Some cavities are as large as 4 cm in diameter and 1 cm in height. Unit 1-B contains smaller pumice lumps which are more collapsed. The pumice lumps of Unit 1-B rarely have a central cavity. The matrix and the pumice lumps of Unit 1-B are both thoroughly indurated, only their colors differing.

Unit 1 contains 8% phenocrysts (Table 8a). Sanidine (72%), quartz (14%), and plagioclase (11%) are the most abundant (Table 8b). Accessory minerals include magnetite (1%), oxyhornblende (1%), and sphene (0.8%).

Sanidine phenocrysts occur as euhedral grains, rounded anhedral grains, polycrystalline grains, and cleavage fragments (Fig. 20). Sanidine also forms rims around plagioclase phenocrysts. The mineral is

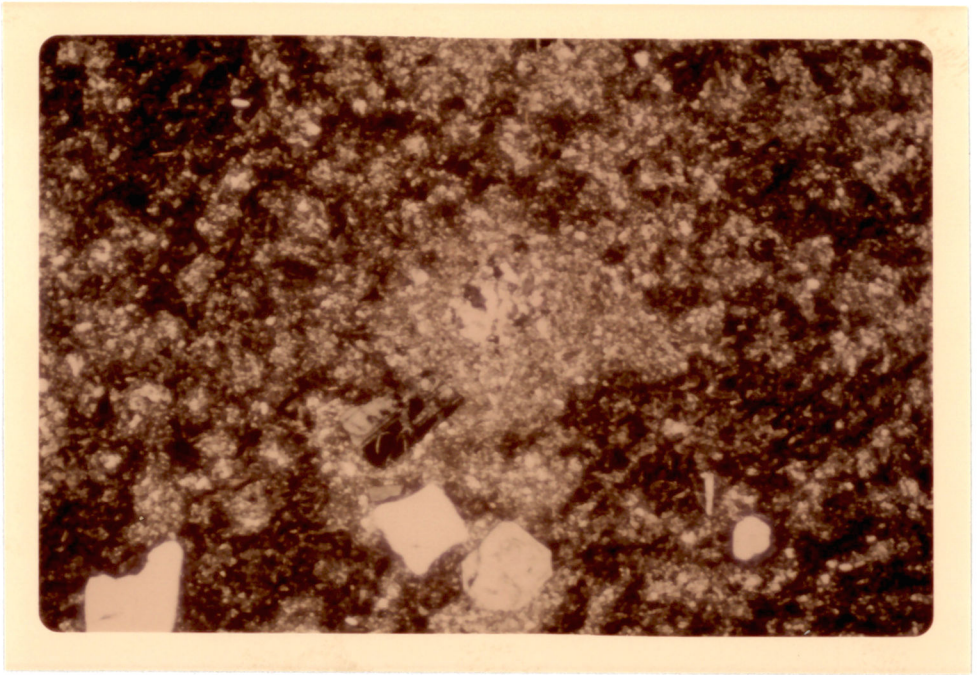

Figure 22. Unit 1-A. Color photomicrograph (crossed nicols) of moderately welded crystal-bearing vitric tuff. The relict pumice lump in the center of the photograph shows an increase in grain size towards the center of the lump. The glass of the pumice lump has undergone granophyric crystallization to sanidine and quartz. The central cavity has been filled with vapor-phase crystals probably of tridymite and sanidine. The dark groundmass (relict shards) has devitrified to spherulites of sanidine and cristobalite (Fig. 21). The four light colored phenocrysts at the bottom of the photograph are sanidine. The phenocryst in the left center of the photograph is plagioclase (An_{29}).

fresh, cleavage cracks are not usually visible, and there are no perthitic intergrowths. Some grains, however, have well developed cleavage and are embayed and/or corroded. The sanidine that rims corroded plagioclase is usually fresh. Sanidine phenocrysts range in size from silt-size up to 5 mm in length but average approximately 1 mm. Sanidine phenocrysts range in composition from Or_{40} to Or_{70} (Table 3). The percentage of sanidine phenocrysts decreases upward in the section, from 80% of the

total phenocrysts in Unit 1-A to 65% of the total phenocrysts in Unit 1-B (Table 8b).

Quartz phenocrysts occur as embayed, rounded grains or irregularly shaped angular fragments. They are relatively devoid of bubbles and solid inclusions and exhibit slight undulatory extinction. The grains range from granule to fine sand-size. The content of quartz phenocrysts is constant throughout Unit 1 (Table 8b).

Plagioclase phenocrysts in Unit 1 are euhedral laths or irregularly shaped angular fragments. Their composition is approximately An_{29} (oligoclase-andesine). The plagioclase is partially resorbed and many grains are rimmed with sanidine. The phenocrysts range from granule to fine sand-size. An increase both in the grain size and the amount of plagioclase occurs upward in the section (4% of phenocrysts in Unit 1-A to 17% in Unit 1-B, Table 8b). The degree of corrosion of grains also decreases toward the top of the section.

Magnetite occurs as euhedral grains, irregularly shaped anhedral grains, and as interstitial dust. Many of the grains are fractured and pitted and are encased in hematite or surrounded by a hematite stained matrix. The magnetite phenocrysts are from coarse sand to silt-size. The content of magnetite is fairly constant throughout Unit 1 (Table 8b).

Oxyhornblende phenocrysts occur as euhedral laths and cleavage fragments. The grains are corroded and poorly preserved. They range in size up to 2 mm in length and constitute about 1% of the phenocrysts (Table 8b).

Sphene occurs as euhedral wedge-shaped grains and as irregularly shaped fragments. The grains are relatively fresh and exhibit slight

pleochroism. The sphene grains, most of which are fine sand-size, are commonly associated with magnetite grains. The content of sphene is fairly consistent in Unit 1 (Table 8b).

Sanidine and quartz were identified by X-ray diffraction as the major rock components and lesser amounts of cristobalite and tridymite (Table 2) were identified.

The sanidine $\bar{2}01$ peaks are split indicating the presence of 2 feldspars. No exsolution lamelli are visible under the microscope, thus the sanidines are cryptoperthites (Bowen and Tuttle, 1950, and Smith, 1974). X-ray analyses of homogenized rock samples are remarkably consistent at about Or_{48} (Table 3). Homogenized sanidine phenocrysts also gave the same composition with the exceptions of sample nos. 1 and 4 (Table 3).

Unit 2

Unit 2-A is a pale reddish brown (10R 5/4) welded tuff with light gray (N7) pumice lumps. Unit 2-B is a light brownish gray (5YR 6/1) welded tuff with light gray (N7) pumice lumps. The unit is a welded vitric tuff (Fig. 9) that contains approximately 86.8% devitrified glass matrix, 12.5% devitrified pumice lumps, and 0.7% phenocrysts (Table 8a).

Relict shard structures are poorly preserved in Unit 2; however, they indicate a high degree of compaction and welding, especially in Unit 2-A (Fig. 23). Relict shard structures are preserved better in Unit 2-A, and some minor post-depositional flowage is indicated (Fig. 24). The original glassy matrix of Unit 2-A crystallized in the form of spherulites (Fig. 25). The spherulites are approximately 1 mm in diameter

Figure 23. Unit 2-A. Color photomicrograph (plane polarized light) of intensely welded vitric tuff (basal vitrophyre). The network of fractures, outlined by hematite, form the boundaries of spherulites and meet in triple-point junctions. The spherulitic fibers are not visible in this photograph, but granular quartz marks the centers of some spherulites and concentric shells are internal subboundaries. The light colored streaks are relict pumice lumps which have been flattened parallel to bedding. Shards have been intensely welded and compacted into the massive dark groundmass which surrounds the relict pumice lumps. Unit 2-A is pale reddish brown (10R 5/4) in hand specimen.

Figure 24. Unit 2-A. Color photomicrograph (plane polarized light) of intensely welded vitric tuff (basal vitrophyre). The light colored streaks are relict pumice lumps and the dark colored streaks are intensely welded relict shards. Post-depositional flowage structures are evident in the photograph. The light colored phenocryst (upper center) is sanidine. A triple-point junction, outlined by hematite, is located in the left center of the photograph. Unit 2-A is pale reddish brown (10R 5/4) in hand specimen.

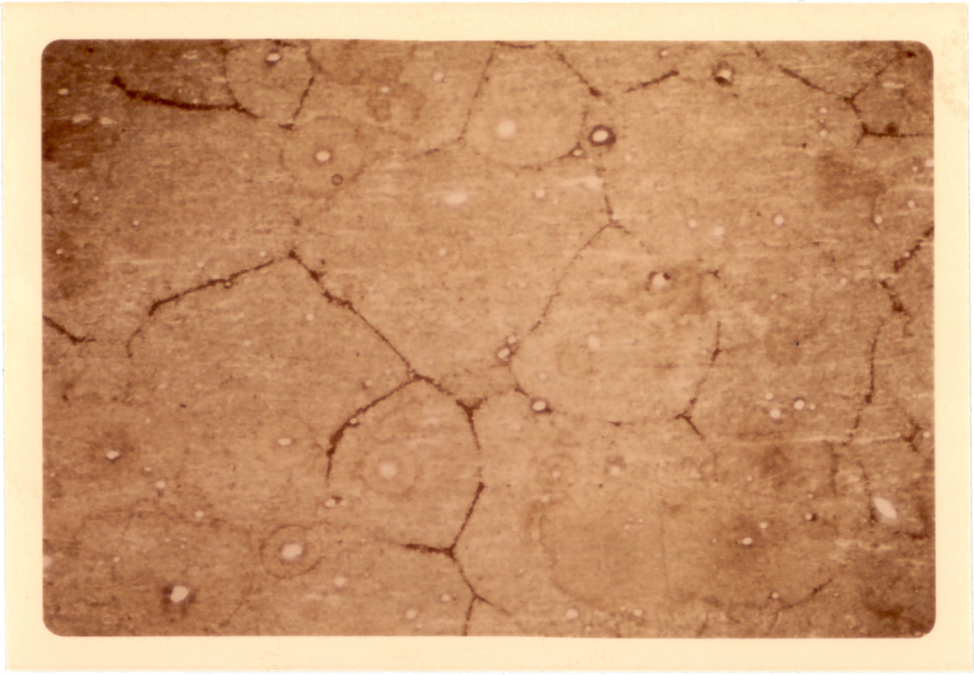

Figure 23

0 0.3
mm

Figure 24

0 0.2
mm

and are commonly outlined by fine fractures that form triple point junctions (Stanton, 1972, Figs. 23 and 24). Some of the spherulites contain small (0.15 mm in diameter) central cavities that are now filled with granular quartz (Fig. 25). The original glassy matrix of Unit 2-B crystallized to form a clay-sized groundmass of equidimensional grains. In the lower portion of Unit 2-B, the groundmass contains poikilitic quartz grains, in optical continuity, that form irregularly shaped but roughly circular areas up to 1 mm in diameter (Fig. 26). The middle and upper portions of Unit 2-B also contain poikilitic quartz, but the grains are smaller and less abundant than in the lower portion of Unit 2-B (Fig. 27).

Most of Unit 2-A is a massive vitrophyre and lacks relict pumice lumps (Fig. 23). Unit 2-B exhibits eutaxitic texture due to flattened, light colored pumice in a dark matrix (Fig. 27). The pumice of Unit 2-B did not completely collapse as did that in Unit 2-A. The pumice lumps form crenulated discs up to 5 cm in diameter and 2 mm in thickness. Their plane of flattening is parallel to bedding. The pumice lumps commonly contain cavities up to 3.5 mm in diameter and 1 mm in height. The cavities are filled or lined with silt-sized vapor-phase crystals (Figs. 26 and 27). The size range of the pumice lumps is consistent throughout Unit 2; however, the amount varies somewhat (Table 7).

Unit 2 contains only 0.7% phenocrysts (Table 8a). Of these, sanidine comprises 88.7% and magnetite 11.3% (Table 8b). Accessory minerals include plagioclase, oxyhornblende, biotite, fayalite, NaFe augite, and zircon.

Sanidine phenocrysts occur as euhedral and round or angular anhedral

Figure 25. Unit 2-A. Color photomicrograph (crossed nicols) of intensely welded vitric tuff (basal vitrophyre). Intensely welded and compacted groundmass of relict pumice lumps and shards produce crude horizontal foliation. The glassy groundmass devitrified into spherulitic structures of sanidine and cristobalite. The center of the spherulite contains granular quartz. The spherulite loses fiber resolution at an internal growth boundary (a). The fractures (b) mark the outer limits of the spherulite. Fractures meet in triple-point junctions (c). Fractures filled to varying degrees with hematite and other unidentified vapor-phase minerals.

Figure 26. Unit 2-B. Color photomicrograph (crossed nicols) of moderately welded vitric tuff from the lower part of Unit 2-B. The relict shards underwent granophyric crystallization to sanidine and poikilitic quartz. Along the lower margin of the photograph is a relict pumice lump which has been flattened and filled with sanidine, tridymite, and other unidentified vapor-phase minerals. The pumice lump underwent granophyric crystallization to sanidine and quartz, but did not crystallize to poikilitic quartz. The boundary (b) is between the relict pumice lump and the groundmass is indistinct. Unit 2-B is light brownish gray (5YR 6/1) in hand specimen.

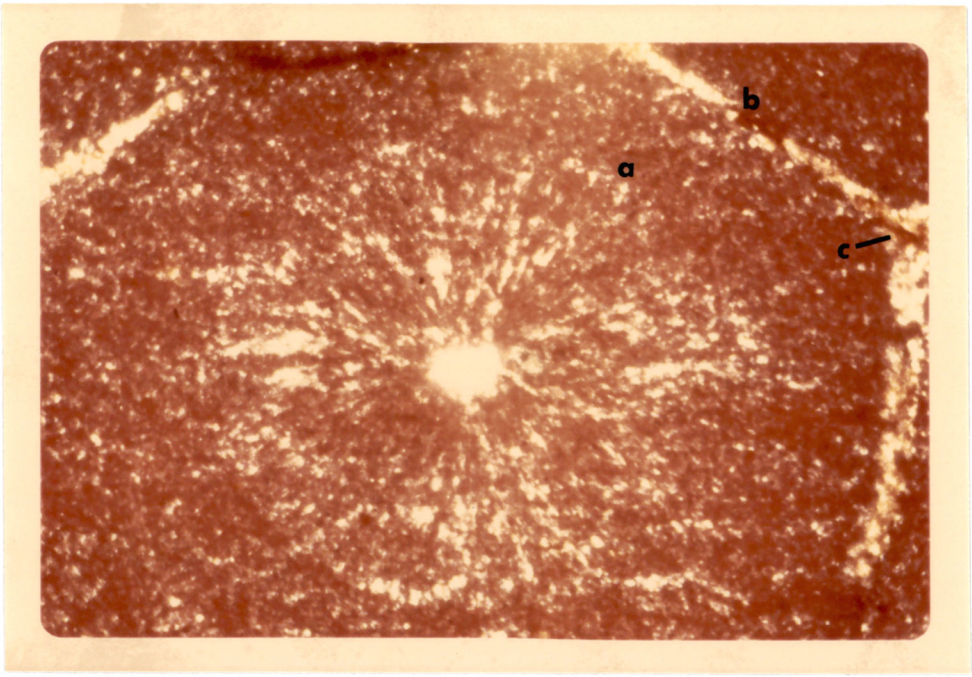

Figure 25

0 0.05
mm

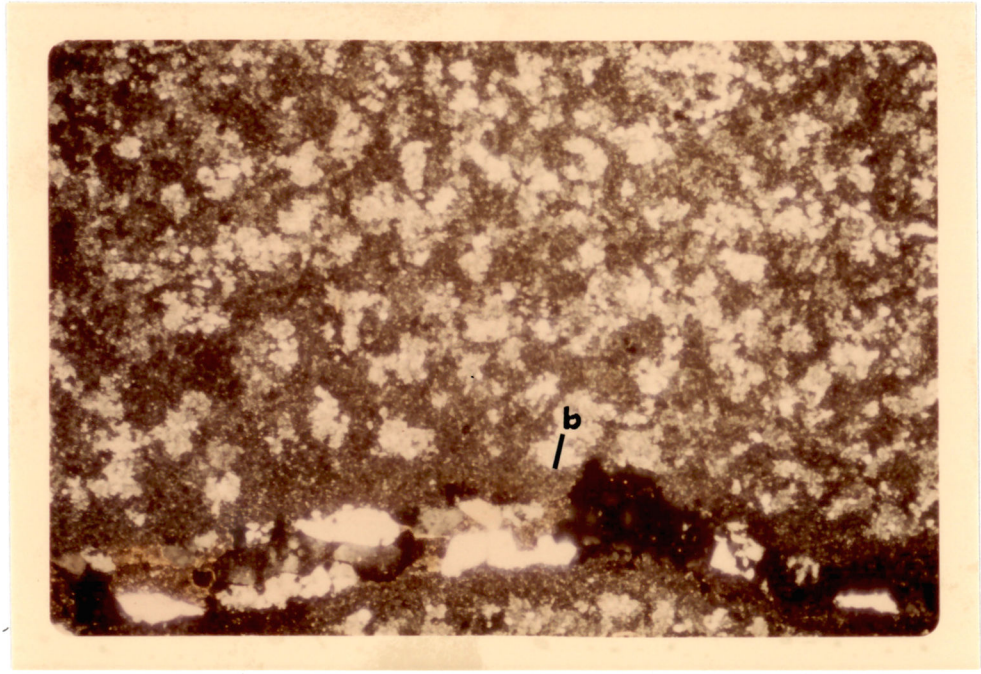

Figure 26

0 0.5
mm

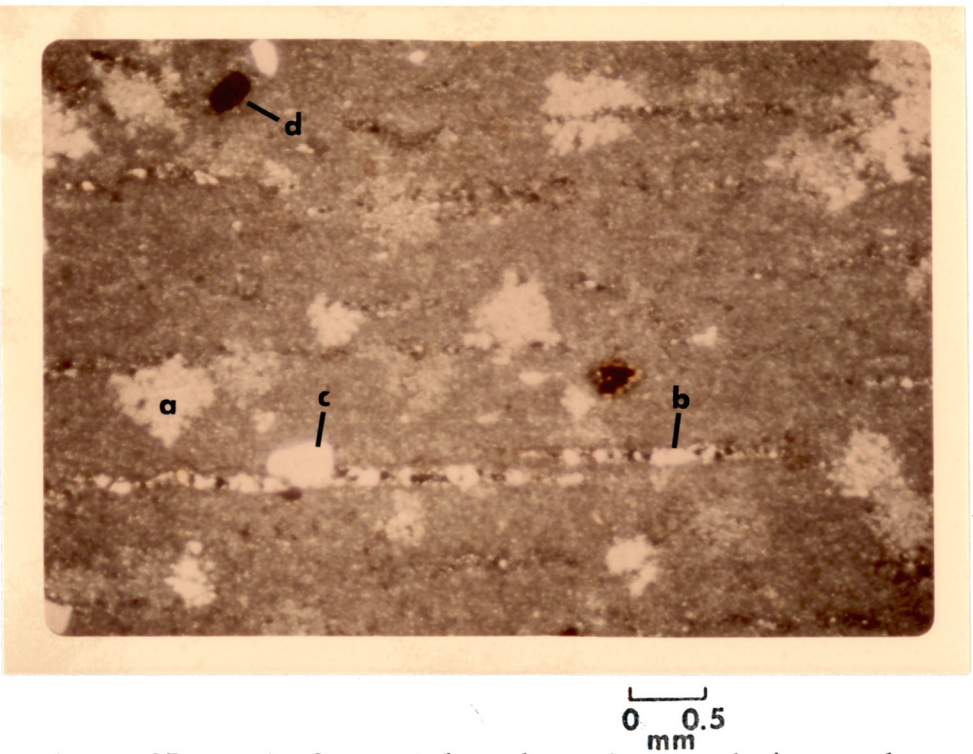

Figure 27. Unit 2-B. Color photomicrograph (crossed nicols) of moderately welded vitric tuff directly below the Unit 2-B — Unit 3 contact. The relict shards devitrified to clay-sized equidimensional grains of sanidine and cristobalite. Some of the relict shards underwent granophyric crystallization to sanidine and poikilitic quartz (a). The flattened relict pumice lumps (b) are filled with vapor-phase sanidine and tridymite crystals. The light colored phenocrysts are sanidine (c) and the opaque phenocrysts are magnetite (d).

grains. The grains average 0.5 mm in length and range up to 2 mm. Cleavage cracks are scarce and the sanidine lacks perthitic intergrowths.

Magnetite grains vary in size up to 0.5 mm in diameter. The phenocrysts are euhedral, rounded, or angular grains. Magnetite is commonly associated with biotite and/or zircon. Magnetite phenocrysts are altered to hematite in varying degrees.

Plagioclase occurs as euhedral grains that have a maximum length of 0.7 mm. Plagioclase composition could not be determined due to the scarcity of grains. A few oxyhornblende phenocrysts are present in

Unit 2. They are usually rimmed with biotite and are up to 0.7 mm in length. Biotite phenocrysts occur in Unit 2 as euhedral grains and range in size up to 0.4 mm in diameter. The biotite is altered and poorly preserved. Fayalite and NaFe augite occur as altered euhedral grains around 0.5 mm in diameter. Zircons occur as fresh euhedral grains usually associated with magnetite.

Sanidine and cristobalite were identified by X-ray diffraction as the major minerals in Unit 2-A (Table 2). Sanidine and quartz were identified as the major minerals of the lower portion of Unit 2-B. Sanidine and cristobalite were identified as the major minerals of the middle and upper portions of Unit 2-B but a significant amount of tridymite also occurs. Sanidine in Unit 2 is a cryptoperthite with a composition of Or_{48} (Table 3).

Unit 3

Unit 3 is a brownish gray (5YR 4/1) welded tuff with light gray (N7) pumice lumps. The rock is a welded vitric tuff (Fig. 9) that contains approximately 64% devitrified glass matrix, 31% devitrified pumice lumps, and 5% phenocrysts (Table 8a).

The shards are poorly preserved but they appear to have been medium sand-size angular plates (Fig. 28). The crystallized glassy matrix consists of randomly orientated, clay-sized, equidimensional grains (Fig. 29) of sanidine and SiO_2 polymorphs (Table 2). The grain size of the groundmass increases slightly upward in the unit. Poikilitic quartz zones occur in Unit 3 and are similar to those in the middle and upper portions of Unit 2-B. These optically continuous quartz zones vary in size up

Figure 28. Unit 3. Color photomicrograph (plane polarized light) of moderately welded, crystal-bearing vitric tuff. Relict shard structures are evident in the areas between phenocrysts and lithic fragments. The phenocrysts are sanidine except for a quartz grain (a) protruding into a cavity of a relict pumice lump. The cavity is lined with vapor-phase tridymite (b). The dark masses along the lower margin of the photograph are lithic fragments. The corroded sanidine phenocryst in the lower left corner of the photograph is contained within a lithic fragment. Lithics are slightly flattened parallel to bedding.

Figure 29. Unit 3. Color photomicrograph (crossed nicols) of moderately welded, crystal-bearing vitric tuff. Relict shards have devitrified to clay-sized, equidimensional grains of sanidine and cristobalite. Cavities in relict pumice lumps are filled with vapor-phase tridymite (wedge-shaped twins), sanidine (tabular grains), and NaFe augite (yellow-colored mineral). Dark spot in lower center of photograph is a hole.

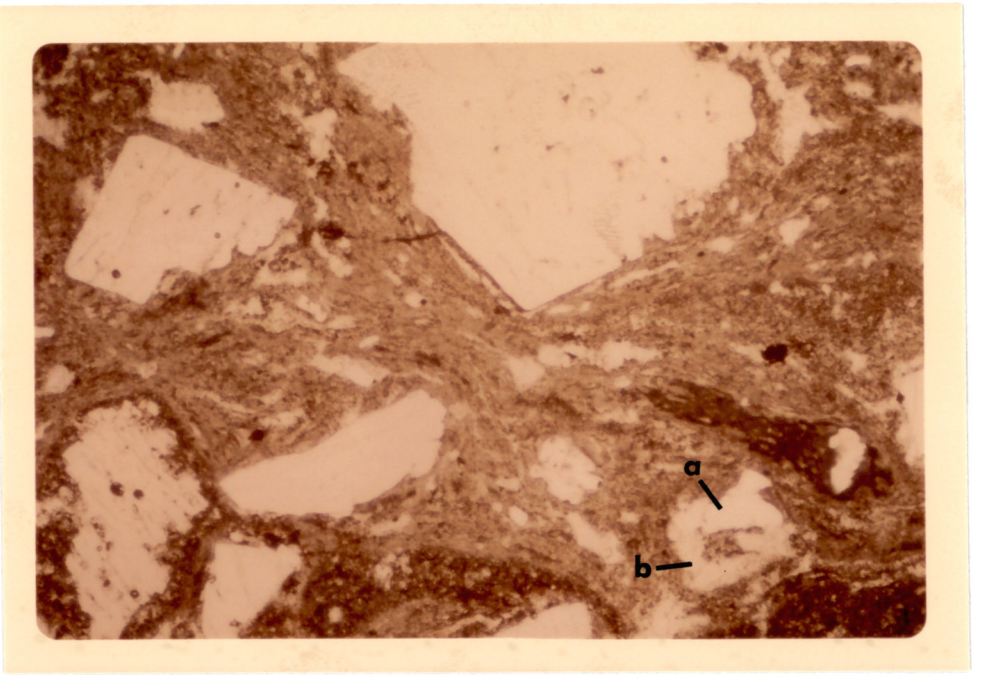

Figure 28

0 0.5
mm

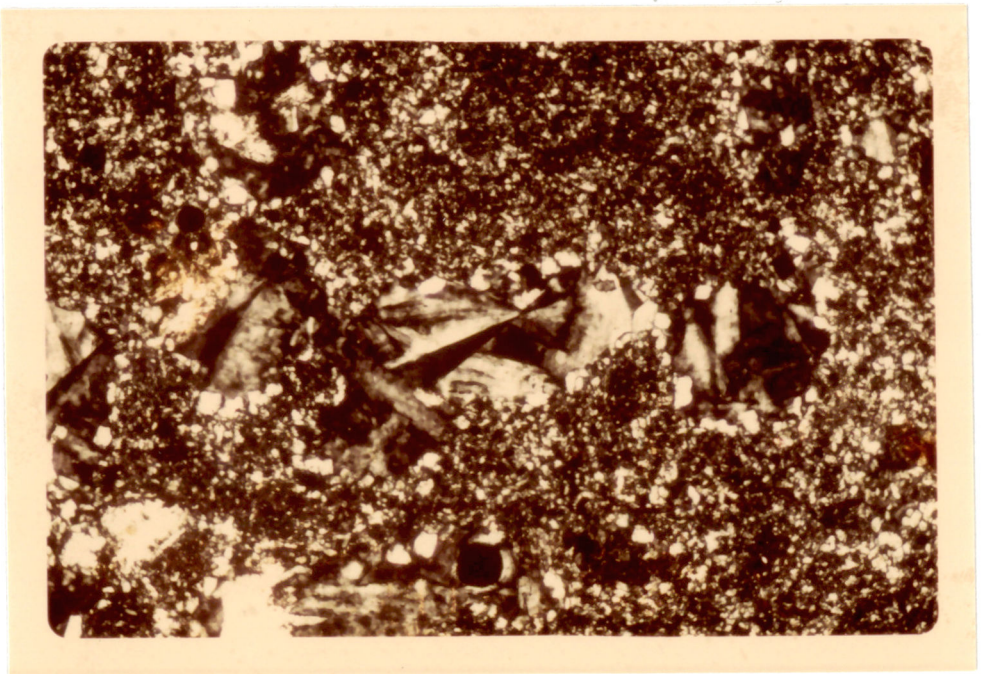

Figure 29

0 0.05

to 0.8 mm in diameter and occur in random fashion in the rock.

The amount of pumice in Unit 3 is constant (Table 7). Eutaxitic texture is developed by highly flattened pumice (Fig. 28) except in the upper 3 m of the unit where pumice lumps are slightly flattened. The change in the degree of compaction is evident in the rock density and porosity data (Figs. 4 and 5). The plane of flattening is parallel to bedding. The pumice lumps form crenulated disc-shaped bodies ranging in size up to 5 cm in diameter and 0.5 cm in height. The upper 3 m of Unit 3 contain less flattened pumice ranging in size up to 4 cm in diameter and 2 cm in height. Open cavities in pumice lumps are less common below this upper portion. Most cavities are lined with silt-sized tridymite crystals (Fig. 29). Magnetite phenocrysts in the pumice lumps are highly altered in the upper 3 m of Unit 3. Botryoidal quartz was precipitated, possibly from groundwater, in some cavities in the upper 3 m of Unit 3.

Phenocrysts, which comprise about 5% of Unit 3 (Table 8a), consist of sanidine (93%), magnetite (5%), and biotite (1.5%) (Table 8b). Accessory minerals include NaFe augite, quartz, fayalite, and zircon. Acmite occurs as phenocrysts in some lithic fragments.

Sanidine occurs as euhedral grains, angular cleavage fragments, round and/or embayed anhedral grains, and polycrystalline grains. The grains range from fine to medium sand-size. The sanidine of Unit 3 is fresh-looking but some grains have been deeply embayed (Fig. 28). A few sanidine grains are zoned crystals and some exhibit exsolution lamelli (microperthites). Cleavage cracks are scarce.

Magnetite occurs as euhedral grains, angular or round anhedral

grains, and polycrystalline grains, which range in size up to 0.5 mm in diameter. Magnetite has undergone varying degrees of alteration to hematite. Biotite phenocrysts in Unit 3 are slightly pleochroic light brownish olive to pale olive, and therefore may be a high magnesium biotite. They occur as small euhedral flakes up to 0.5 mm in diameter. Biotite also commonly occurs as a rim on highly altered NaFe augite phenocrysts. NaFe augite phenocrysts occur as highly altered lath-shaped grains up to 1 mm in length. Quartz phenocrysts occur as round and/or embayed anhedral grains up to 0.5 mm in diameter. Fayalite phenocrysts are pale green and are associated with mafic minerals. Grain morphology varies from euhedral to round or angular anhedral grains. They exhibit the characteristic curved fractures of olivine. Zircon phenocrysts occur as euhedral grains usually encased or associated with magnetite. The grains, which are as large as 0.5 mm in length, average about 0.2 mm. Acmite occurs only as phenocrysts in lithic fragments. The grains are fresh and average about 0.15 mm in length. The phenocrysts exhibit good pleochroism and the characteristic pyroxene cleavage. Acmite occurs as euhedral grains and as round and/or embayed grains.

The lithic fragments of Unit 3 comprise about 4% of the rock (Table 7). They are darker in color than the groundmass and flattened into disc-shaped bodies with their plane of flattening parallel to bedding. The lithic fragments are primarily a less felsic, vesicular, porphyritic, aphanitic, volcanic rock. The predominant phenocryst contained in these lithic fragments is acmite (Fig. 28). In the upper 3 m of Unit 3 where the degree of compaction is less, the lithic fragments are commonly vesicular and not flattened.

Botryoidal quartz occurs in some cavities of the upper 3 m of Unit 3 similar to those shown in Unit 4. The quartz grains form radial and concentric patterns. Usually the quartz infillings consist of several stages of growth with truncated structures.

Sanidine and cristobalite were identified by X-ray diffraction analysis as the major minerals comprising Unit 3 (Table 2), however tridymite increases in abundance upward in Unit 3. Groundmass and phenocryst sanidines are mostly cryptoperthites. The composition of about Or_{48} is consistent with sanidines in the other ignimbrites (Table 3).

Unit 4

Unit 4 is a light brownish gray (5YR 6/1) at the base and grayish red (10R 4/2) at the top. The pumice lumps are light gray (N7) and the lithic fragments are brownish gray (5YR 4/1). The unit is a welded lithic tuff (Fig. 9) which consists of 51% ash-size material (small lithic fragments and devitrified glass), 20% devitrified pumice, 21% lapilli-sized, lithic fragments, and 7% phenocrysts (Table 8a). The ash-sized component consists predominantly of small lithic fragments with minor amounts of devitrified shards (Fig. 30). Weak compaction and deformation of lithic fragments have developed a crude foliation in the rock.

Eutaxitic texture is developed by pumice lumps and lithic fragments. The pumice lumps are flattened into disc-shaped bodies with their plane of flattening parallel to bedding. The pumice lumps are as large as 2 cm in diameter and 0.5 cm in thickness. Open cavities up to 2 cm in diameter

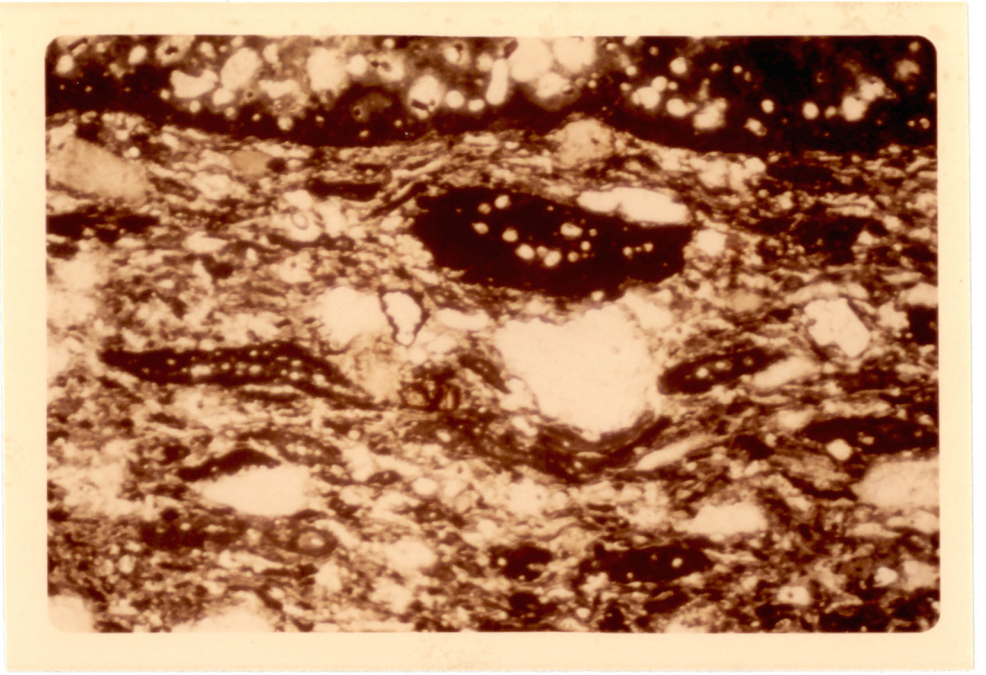

Figure 30. Unit 4. Color photomicrograph (plane polarized light) of moderately welded lithic tuff. Eutaxitic texture was developed by compression of lithic fragments and pumice lumps. The lithic fragments range from clay- to gravel-size. The large lithic fragments, like the one along the upper margin of the photograph, are vesicular and contain acmite phenocrysts (small orange grains). The light colored phenocrysts are sanidine. The brown colored phenocryst in the center of the photograph is NaFe augite.

occur in many pumice lumps. These cavities are lined with silt-sized vapor-phase sanidine crystals (Fig. 31) and a few of the cavities are filled with botryoidal quartz (Fig. 32). The pumice has crystallized to a silt-sized mosaic (Fig. 31) of equidimensional grains of sanidine and SiO_2 polymorphs similar to the pumice lumps of Unit 1 (Fig. 22).

Lithic fragments in the ash-to lapilli-size range constitute about 70% of the deposit. The lithic fragments are vesicular, porphyritic, aphanitic, volcanic rock fragments that are less felsic than the vitric components of the rock. The larger lithic fragments, sand-to lapilli-

Figure 31. Unit 4. Color photomicrograph (crossed nicols) of moderately welded lithic tuff showing a relict pumice lump. The pumice has crystallized to equidimensional grains of sanidine and a polymorph of SiO_2. Grain size increases from the pumice lump - groundmass boundary towards the center. Tabular vapor-phase sanidine crystals project into the central cavity of the relict pumice lump.

Figure 32. Unit 4. Color photomicrograph (plane polarized light) of a relict pumice lump in moderately welded lithic tuff. The egg-shaped relict pumice lump is in sharp contact (a) with the dark groundmass. Vapor-phase crystals and crystallized pumice glass have been partially removed, probably by ground water, and are in sharp contact (b) with the botryoidal quartz infilling. The radial fibers are quartz crystals and the concentric bands (c) are growth boundaries which were coated with impurities.

Figure 31

0 0.05
mm

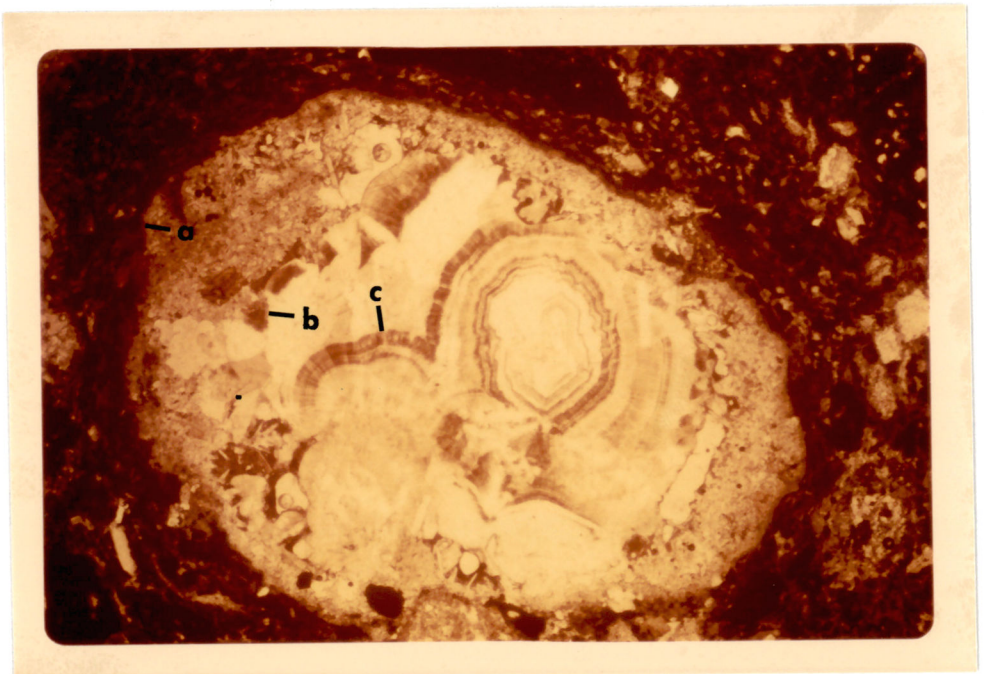

Figure 32

0 0.5
mm

size, are usually vesicular and many contain acmite and magnetite phenocrysts (Fig. 30). Some fragments are slightly flattened with their plane of flattening parallel to bedding. A less abundant type of lithic fragment in Unit 4 is a light gray porphyritic, aphanitic volcanic rock with silt-sized tabular sanidine phenocrysts.

The phenocrysts of Unit 4 comprise about 7% of the unit (Table 8a). Of these, sanidine constitutes 98%, magnetite 1%, and amphibole 1% (Table 8b). Accessory phenocrysts include fayalite, NaFe augite, and zircon. Acmite phenocrysts occur only in the predominant lithic fragment type.

Sanidine occurs as euhedral, round or angular anhedral, and polycrystalline grains that range from fine to coarse sand-size. Most of the grains are embayed and/or pitted. Some grains exhibit cleavage cracks and some exhibit perthitic intergrowths (microperthite).

Magnetite phenocrysts occur as euhedral, round or angular anhedral, and polycrystalline grains. The grains range in size up to 0.5 mm in diameter. Most magnetite is altered, to varying degrees, to hematite. Amphibole occurs as highly altered lath-shaped phenocrysts up to 0.5 mm in length. They are usually rimmed with biotite. Fayalite phenocrysts in Unit 4 are poorly preserved but the characteristic curved cracks and pale green color are diagnostic. The grains are circular in cross section and as large as 0.5 mm in diameter. NaFe augite occurs as altered lath-shaped grains up to 1 mm in length (Fig. 30). Zircon occurs as minute euhedral grains usually associated with magnetite. The phenocrysts rarely exceed 0.2 mm in length. Acmite occurs only as phenocrysts in the predominant lithic fragments (Fig. 30). The acmite grains

are well preserved and they rarely exceed 0.15 mm in length. The phenocrysts exhibit the characteristic pleochroism and pyroxene cleavage of acmite and occur as euhedral grains and round and/or embayed anhedral grains.

Botryoidal quartz fills some cavities in Unit 4 (Fig. 32). Vapor-phase crystals and crystallized pumice glass are partially removed from the cavities which are filled with botryoidal quartz. The quartz grains form radial and concentric patterns and the quartz infillings usually consist of several stages of growth with truncated structures.

Sanidine and cristobalite were identified by X-ray diffraction as the major minerals comprising Unit 4 (Table 2). Groundmass and phenocryst sanidines are mostly cryptoperthites with a composition of about Or_{48}, similar to sanidine in the other ignimbrites (Table 3).

Unit 5

Unit 5 consists of a grayish orange-pink (10R 8/2) altered, unwelded, vitric tuff which grades upward into a light gray (N7) moderately welded, vitric-lithic tuff. The unwelded basal tuff was composed predominantly of shards, pumice lumps, and sanidine and magnetite phenocrysts. Most of the ash and pumice has been altered to a smectite-group clay but some glass is still present. Primary structures are well preserved in some pumice lumps; however, shards are not well preserved. The moderately welded vitric-lithic tuff (Fig. 9) consists of 71% devitrified glassy matrix, 15% devitrified pumice, 12% lithic fragments, and 2% phenocrysts (Table 8a).

Relict shards (Fig. 33a) were elongate plates and wedges of medium sand-size. They have been pressed together and welded but were not highly deformed. Shards were highly deformed around rigid objects like lithic fragments, phenocrysts, and to a lesser extent, around pumice lumps. The glass crystallized to a clay-sized mosaic of equidimensional grains (Fig. 33b) of sanidine and SiO_2 polymorphs (Table 2). Some shards crystallized with axiolitic structures.

Eutaxitic texture in Unit 5 is the result of pumice lumps that are slightly to highly flattened parallel to bedding. The pumice crystallized to silt-sized equidimensional grains (Fig. 33b) of sanidine and SiO_2 polymorphs similar to the texture of crystallized pumice lumps in Unit 1 (Fig. 22) and Unit 4 (Fig. 31). The silt-sized grains are between the pumice lump-groundmass boundary and the axiolitic portion of the pumice lump. Central cavities commonly occur in pumice lumps and they are lined or filled with silt-sized, vapor-phase crystals (Fig. 31).

The phenocrysts make up about 2% of Unit 5 (Table 8a), and sanidine is the predominant phenocryst (Table 8b). Accessory minerals include magetite and oxyhornblende.

Sanidine phenocrysts occur as euhedral grains, round and/or embayed anhedral grains, angular cleavage fragments, and polycrystalline grains. The grains range from coarse to fine sand-size. Cleavage cracks are scarce and perthitic intergrowths are not present.

Magnetite occurs as euhedral and round or angular anhedral grains. Grains range in size up to 0.5 mm in diameter and are slightly altered to hematite. Oxyhornblende phenocrysts occur as euhedral laths up to 1 mm in length.

Figure 33a. Unit 5. Color photomicrograph (plane polarized light) of moderately welded, vitric-lithic tuff. Relict shard structures are evident. The relict pumice lump (center of photograph) has crystallized to equidimensional grains (a) and axiolitic structures (b) of sanidine and SiO_2 polymorphs (see Figure 33b). The central cavity (c) is filled with vapor-phase minerals. Hematite marks the boundary (d) between the pumice lump and the groundmass. Hematite or magnetite (altered to hematite) dust probably coated the pumice lump prior to deposition. The light, tabular (euhedral) phenocryst is sanidine. Unit 5 is light gray (N7) in hand specimen.

Figure 33b. Unit 5. Color photomicrograph (same as Figure 33a except crossed nicols) of moderately welded, vitric-lithic tuff. Relict shards have devitrified to equidimensional grains of sanidine and cristobalite.

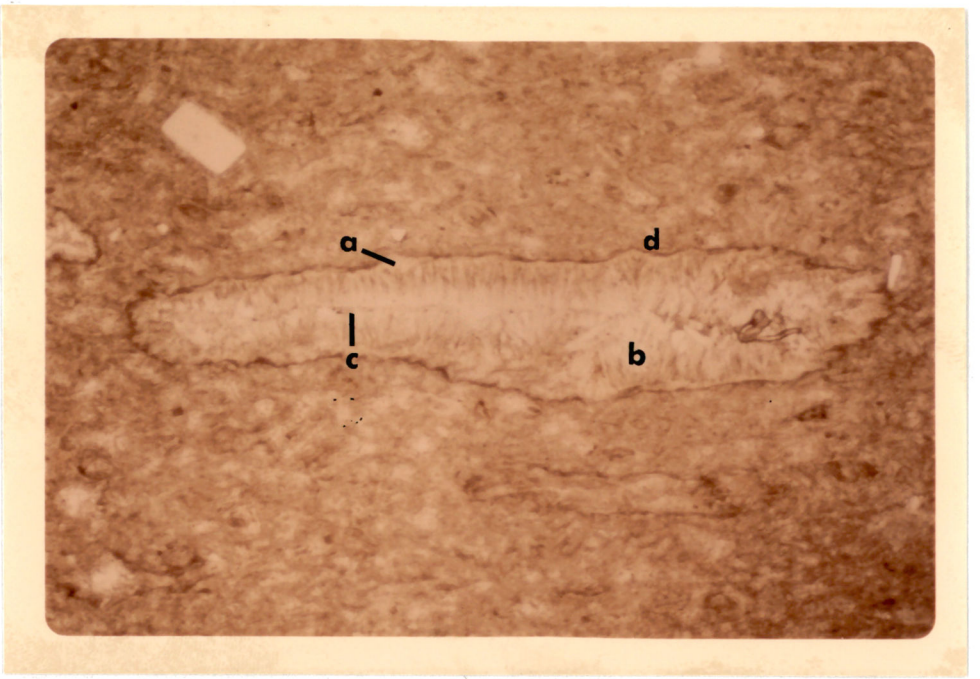

Figure 33a

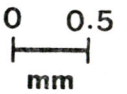

Figure 33b

Sanidine, cristobalite, and quartz were identified by X-ray analysis as the major minerals comprising the welded portions of Unit 5 (Table 2). The altered basal tuff contains a smectite-group clay which was identified by its basal d-spacing of about 16Å. Sanidine in Unit 5 is a cryptoperthite with a composition of about Or_{51} (Table 3), similar to that in the other ignimbrites. The composition of sanidine phenocrysts in Unit 5 is Or_{39} (Table 3).

MAJOR ELEMENTAL ANALYSIS

Data Processing

Counting rates of over 10,000 counts/second were corrected for counter dead time using:

$$N = N'/1 - N'\tau,$$

where N is the true counting rate, N' is the observed counting rate, and τ is the counter dead time of 3.6 microseconds (Hutchison, 1974).

The counts were adjusted for sample position. Test position nos. 3 and 4 were standardized to position no. 2 because the same pellet tested in positions 2, 3, and 4 gave slightly different counting rates.

The peak and two background counting rates were determined for each element (Table 5). The two background values were averaged and subtracted from the peak value to give true intensity. Graphical methods were used to determine the background for calcium because of interference by the tail of the potassium K_β peak. Only one background for aluminum could be obtained since its peak is at a 2θ of 144.65° and the goniometer will not rotate beyond a 2θ of 145°.

The equation which relates the measured intensity (I) of an element to its weight percent (W) is:

$$1)\ I = \mu(W),$$

where μ is the absorption coefficient of the sample for the wavelength of a given characteristic line. The equation which relates the intensity ratios for a given element in the sample and the standard to weight percent ratios is:

$$2)\ \frac{I_{sam}}{I_{std}} = \frac{\mu_{sam}(W_{sam})}{\mu_{std}(W_{std})}.$$

When the bulk chemical compositions of the sample and standard are similar, then their absorption coefficients are also approximately equal and can be dropped from equation 2 (Hutchison, 1974). Then equation 2 becomes:

$$3)\ \frac{I_{sam}}{I_{std}} = \frac{W_{sam}}{W_{std}}.$$

The weight percentages were adjusted to a total of 99%. This is the total weight percentages for the major elements in sample no. 5 (Table 9) and is assumed to approximate the sum of the weight percentages of elements for the other ignimbrites. The weight percentages of sample no. 5 (Table 9) were corrected for absorption and differ as follows: Al_2O_3 is high by 9%, and K_2O is low by 6%. Both these corrections would make the alumina saturation index slightly less than those shown in Table 14.

Sodium percentages were not determined using the X-ray spectrometer, but were calculated (Table 11) using K_2O weight percentages (Table 10) and Or percentage values of sanidine (Table 3). The ignimbrites are composed primarily of sanidine ($[Na,K]AlSi_3O_8$) and SiO_2 polymorphs

OXIDE	SiO_2	Al_2O_3	K_2O	Na_2O	CaO	Fe_2O_3	TiO_2
Sample no. 5 with absorption correction	76.5	11.2	5.1	3.4	0.4	1.3	0.2
Sample no. 5 without absorption correction	76.5	12.1	4.8	3.2	0.4	1.0	0.2
Difference	0	0.9	0.3	0.2	0	0.3	0

Table 9. Oxide weight percentages for sample no. 5 determined with and without a correction for matrix absorption. Na_2O percentages determined by using K_2O values and Or content of the sanidine.

(Table 2) so that almost all of the sodium and potassium are in sanidine. The Na/K ratio in sanidine is thus a good approximation of the Na/K ratio in the rock. Na_2O analyses were (Table 10) performed on the samples by atomic absorption following an $HF-HNO_3-HClO_4$ digestion of a 0.1 g sample (Post, 1976, personal communication).

The fluorescence analysis was repeated on sample no. 9 to check reproducibility (Table 12). The weight percentages check to within 0.4% for SiO_2 and to within 0.2% for the other oxides.

Ignimbrite Petrochemistry

Units 1, 2, 3, and 5 contain SiO_2 contents of 76.5%, 75.5%, 73.7%, and 76.2% (Table 13); therefore, they are high silica rhyolites (Christiansen and Lipman, 1972). The lower SiO_2 content in Unit 4 (71%) is the result of a lower SiO_2 content in the lithic fragments.

Shand's (1969) classification of Al_2O_3 saturation is based on molecular proportions of Al_2O_3 to the sum of Na_2O, K_2O, and CaO. The Al_2O_3

	OXIDE	SiO_2	Al_2O_3	K_2O	$Na_2O_{(L)}$	CaO	Fe_2O_3	TiO_2
	22	76.1	11.9	5.2	3.6	0.2	1.1	0.1
	21	58.2	28.9	0.8	n.d.	2.1	3.1	0.4
	20	70.6	13.2	5.8	3.7*	1.0	3.7	0.6
	19	71.3	12.6	5.6	3.7*	1.0	3.4	0.5
	18	75.7	11.1	4.8	3.1	0.4	2.6	0.3
	17	74.5	11.7	5.2	3.6	0.4	2.7	0.3
	16	73.6	12.2	5.3	3.9	0.4	2.8	0.3
	15	72.8	12.6	5.4	3.5	0.5	3.0	0.3
	14	71.4	13.1	5.7	4.2	0.5	3.3	0.4
S								
A	12	75.7	11.5	4.7	3.4	0.2	2.7	0.2
M								
P	11	75.6	11.5	4.8	3.4	0.2	2.7	0.2
L								
E	10	74.9	12.1	5.0	3.4	0.3	2.5	0.2
	9	75.2	11.5	5.0	3.1	0.3	2.7	0.2
	8	75.6	11.4	5.1	3.4	0.2	2.7	0.2
	7	75.5	11.4	4.9	3.1	0.3	2.7	0.2
	6	75.8	12.2	5.1	3.2	0.4	1.1	0.2
	5	76.5	12.1	4.8	3.8	0.4	1.0	0.2
	4	76.3	12.2	4.8	3.8	0.5	1.0	0.2
	3	76.8	11.3	4.5	3.1	0.8	1.0	0.2
	2	76.4	12.4	4.8	3.5	0.5	1.0	0.2
	1	76.4	12.6	4.5	3.1	0.4	1.0	0.2

Table 10. Oxide weight percentages of major elements in the ignimbrites near Sacramento, Chihuahua, Mexico. SiO_2, Al_2O_3, K_2O, CaO, Fe_2O_3 ($FeO + Fe_2O_3$), and TiO_2 weight percentages determined by X-ray fluorescence. $Na_2O_{(L)}$ weight percentages determined by atomic absorption. * - Na_2O percentage estimated by the weight percent K_2O and Or content of the sanidine.

		$Na_2O_{(L)}$ Atomic Absorption	Na_2O Estimated	Difference
	22	3.6	3.5	-0.1
	18	3.1	3.2	+0.1
	17	3.6	3.4	-0.2
	16	3.9	3.5	-0.4
	15	3.5	3.6	+0.1
S	14	4.2	3.8	-0.4
A				
M	12	3.4	3.1	-0.3
P	11	3.4	3.2	-0.2
L	10	3.4	3.3	-0.1
E	9	3.1	3.3	+0.2
	8	3.4	3.1	-0.3
	7	3.1	3.2	+0.1
	6	3.2	3.3	+0.1
	5	3.8	3.2	-0.6
	4	3.8	3.2	-0.6
	3	3.1	3.2	+0.1
	2	3.5	3.1	-0.4
	1	3.1	3.0	-0.1

Table 11. Na_2O weight percentages for the ignimbrites near Sacramento, Chihuahua, Mexico, determined by atomic absorption analysis and estimated by the weight percent K_2O and Or content of the sanidine. Most estimated values are slightly lower than the values determined by atomic absorption because estimated values are based on the assumption that all K_2O and Na_2O are contained in sanidine.

	OXIDE	SiO_2	Al_2O_3	K_2O	CaO	Fe_2O_3	TiO_2
S	9	75.2	11.5	5.0	0.3	2.7	0.2
A							
M	9						
P	Recheck	75.6	11.3	4.9	0.3	2.6	0.2
L							
E	Difference	0.4	0.2	0.1	0	0.1	0

Table 12. Oxide weight percentage of sample no. 9 of the ignimbrites from the section near Sacramento, Chihuahua, Mexico. The values, determined by two separate runs on the X-ray spectrometer, show a difference of 0.4% for SiO_2 and less than 0.2% for the other oxides.

saturation indices are listed as follows:

peraluminous - $Al_2O_3 > Na_2O+K_2O+CaO$,
metaluminous - $Al_2O_3 > Na_2O+K_2O$, but $Al_2O_3 < Na_2O+K_2O+CaO$,
subaluminous - $Al_2O_3 \leq Na_2O+K_2O+CaO$, and
peralkaline - $Al_2O_3 < Na_2O+K_2O$.

The chemical compositions of the units are such that their Al_2O_3/Na_2O+K_2O+CaO mole ratios are approximately 1.0 (Table 14). For this reason, the ignimbrites are considered to be on the border between subaluminous and peralkaline types. This conclusion is reinforced by mineralogic data. The major minerals are sanidine ($[Na,K]AlSi_3O_8$) and SiO_2 polymorphs with only very small amounts of other Al_2O_3-, Na_2O-, K_2O-, and CaO-bearing minerals occurring. The Al_2O_3/Na_2O+K_2O+CaO mole ratio of sanidine is also 1.0. Mineralogically the ignimbrites are alkali rhyolites because of the predominance of sanidine and polymorphs of SiO_2 (Sorensen, 1974).

OXIDE		SiO_2	Al_2O_3	K_2O	$Na_2O_{(L)}$	CaO	Fe_2O_3	TiO_2
	5	76.1	11.3	5.2	3.6	0.3	1.1	0.2
U	4	71.0	12.9	5.7	3.7*	1.0	3.6	0.5
N								
I	3	73.6	12.2	5.3	3.7	0.4	2.9	0.3
T								
	2	75.4	11.6	4.9	3.3	0.2	2.6	0.2
	1	76.4	12.1	4.8	3.4	0.5	1.0	0.2

Table 13. Average oxide weight percentages for major elements in the ignimbrite units near Sacramento, Chihuahua, Mexico. $Na_2O_{(L)}$ determined by atomic absorption and the others by X-ray fluorescence. * - Na_2O percentage estimated by the weight percent K_2O and Or content of the sanidine.

OXIDE		Al_2O_3	K_2O	Na_2O	CaO	Al_2O_3/K_2O+Na_2O+CaO
	5	0.1109	0.0552	0.0581	0.0053	0.935
U	4	0.1265	0.0605	0.0597	0.0177	0.917
N						
I	3	0.1194	0.0563	0.0597	0.0071	0.970
T						
	2	0.1134	0.0520	0.0532	0.0035	1.043
	1	0.1187	0.0509	0.0548	0.0089	1.036

Table 14. Oxide mole fractions and Al_2O_3/K_2O+Na_2O+CaO mole ratios for the ignimbrite units near Sacramento, Chihuahua, Mexico.

COOLING UNITS

Introduction

Ash flows have sufficiently low viscosities that they can form extensive ignimbrite shields or sheet-type deposits. Ash flows commonly are erupted from linear and arcuate fissures and are associated with caldera structures that form as the surface rocks collapse into the magma chamber as support is removed due to the eruption of magma (Macdonald, 1972).

Ash-sized material is generated by extreme frothing of gas-rich magma in the vent (Fig. 34) where confining pressures decrease sufficiently allowing expansion to occur (Macdonald, 1972). As the gases expand, the magma is first inflated to pumice, and then torn apart to form angular shards. The shards form as Y-shaped septa or plates which separated adjoining bubbles in the froth. The portion of the froth which is not disrupted is preserved as pumice. The emulsion of gas, shards, pumice, phenocrysts, and lithic fragments rises to the lip of

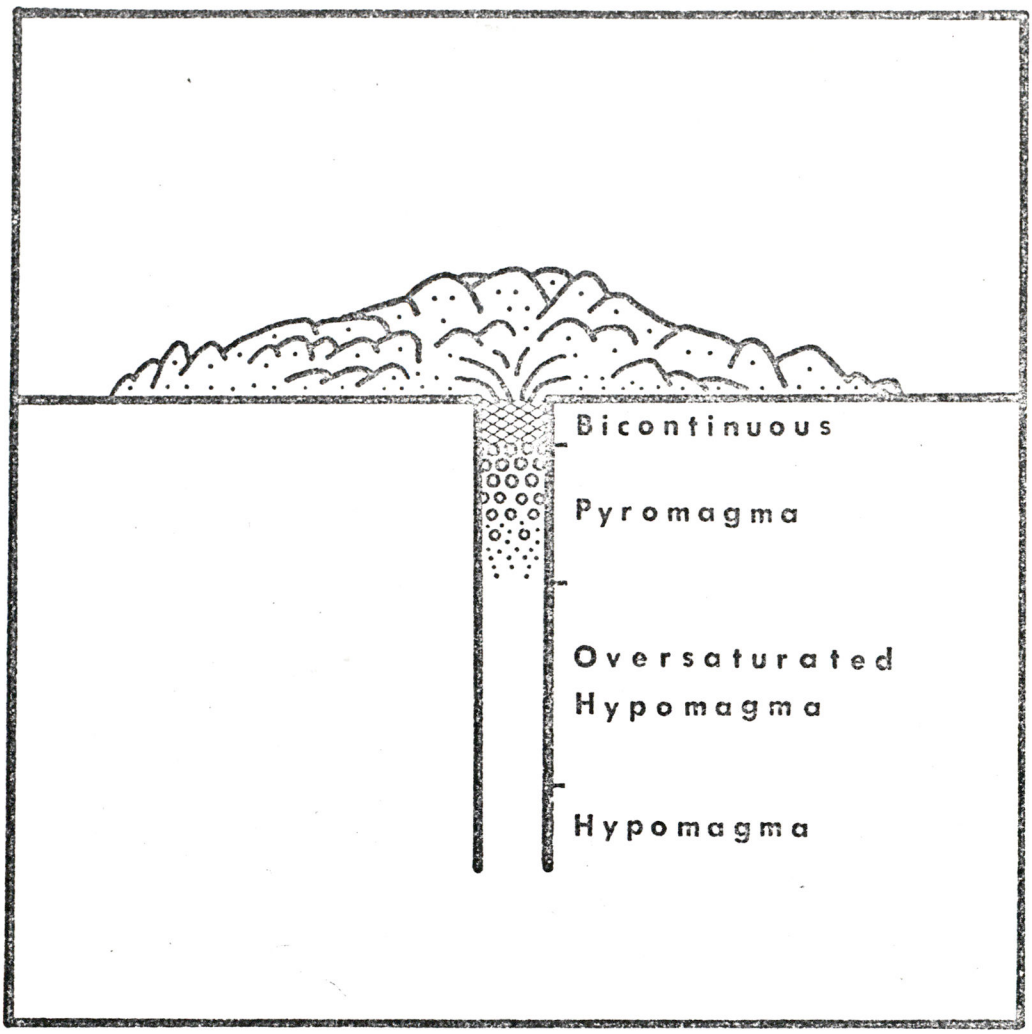

Figure 34. Interpretation of an ash-flow eruption. The hypomagma is saturated or undersaturated with gas. As the magma rises into zones of lower pressure, it becomes oversaturated and bubbles start to form (pyromagma). Bubble walls rupture (bicontinuous zone) and form shards. Inflated magma which does not get torn apart forms pumice. The shallow explosion level results in an overflow of the gas-and-ash mixture. The higher the viscosity of the magma, the shallower the explosion level; hence the more viscous, siliceous magmas are more apt to produce ash flows than are the less viscous, basic magmas (from Macdonald, 1972).

the vent and then simply overflows. The particles in the flow are cushioned by expanding gases which sometimes are still being emitted by the vitric particles (autoexplosivity). Rapid extrusion of vast amounts of material results in burial of the existing topography and the deposits commonly form nearly level upper surfaces. In most cases there is only minor cooling of a moving ash flow because there is little mixing of the particle-rich phase of the cloud with the atmosphere. The homogeneity of the deposit results from the high turbulence in the cloud which causes continuous mixing of particles until the cloud stops moving (Macdonald, 1972). Deposition from the cloud occurs when particles enter the zone of low velocity close to the ground. Changes in an ignimbrite occur following deposition. The particles respond to load pressure, high temperature, and gas activity, which produce varying degrees of compaction, welding, vapor-phase crystallization, devitrification, granophyric crystallization, and oxidation (Fig. 35).

A cooling unit is a flow or series of flows that cool as a single unit. Most single flows are single cooling units. However, two or more ash flows that accumulate rapidly develop the post-depositional changes that are characteristic of single cooling units. This occurs when the ash flows are erupted in rapid succession so that the deposit achieves a uniform temperature and cools as a single unit.

Unit 1

Unit 1 is a single flow and cooling unit. The deposit was relatively thick initially, because the measured section is 100 m thick and the lower and uppermost portions of the ignimbrite are missing (Fig. 11).

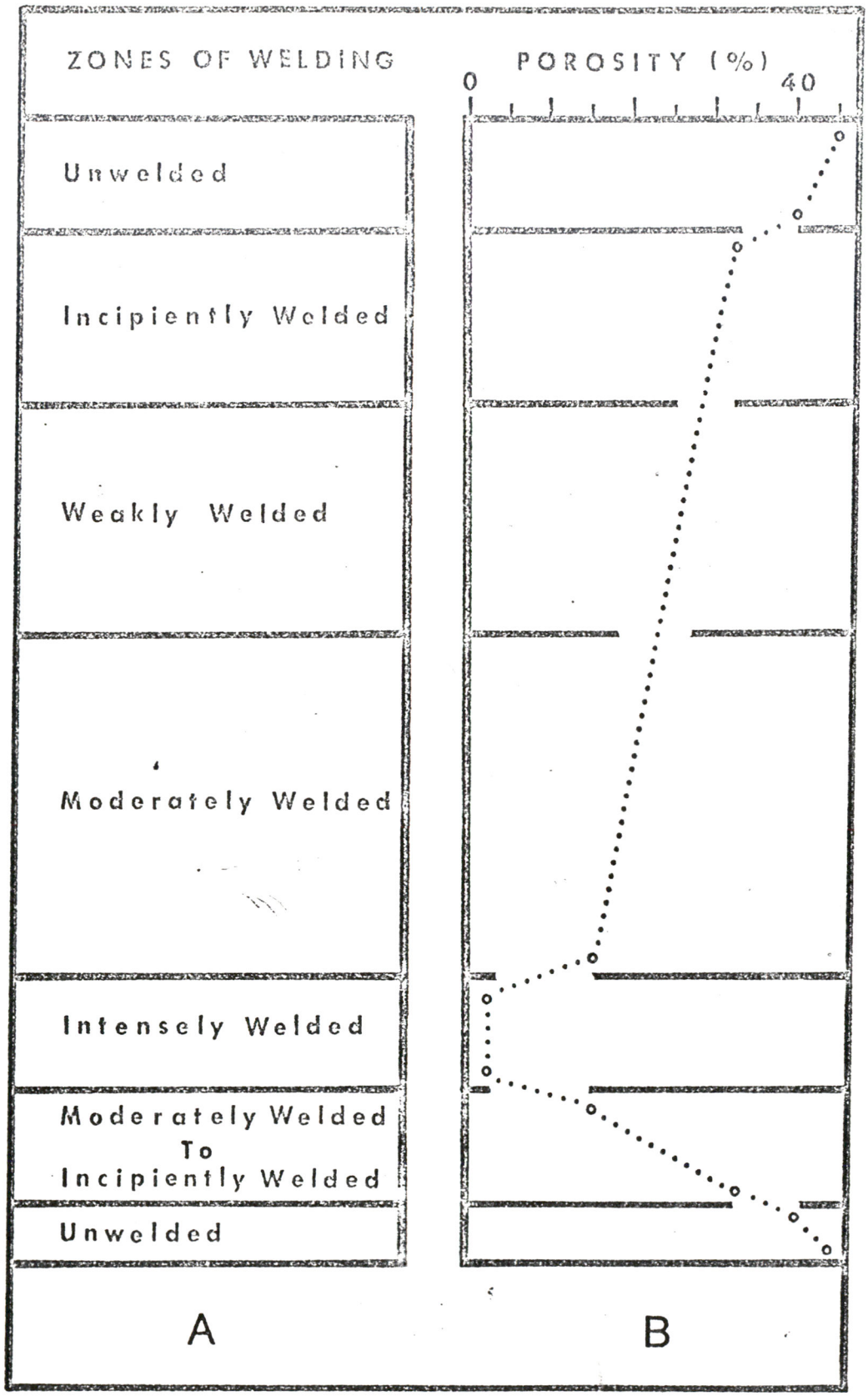
ZONES OF WELDING
POROSITY (%)
0
40
Unwelded
Incipiently Welded
Weakly Welded
Moderately Welded
Intensely Welded
Moderately Welded To Incipiently Welded
Unwelded
A
B

Figure 35

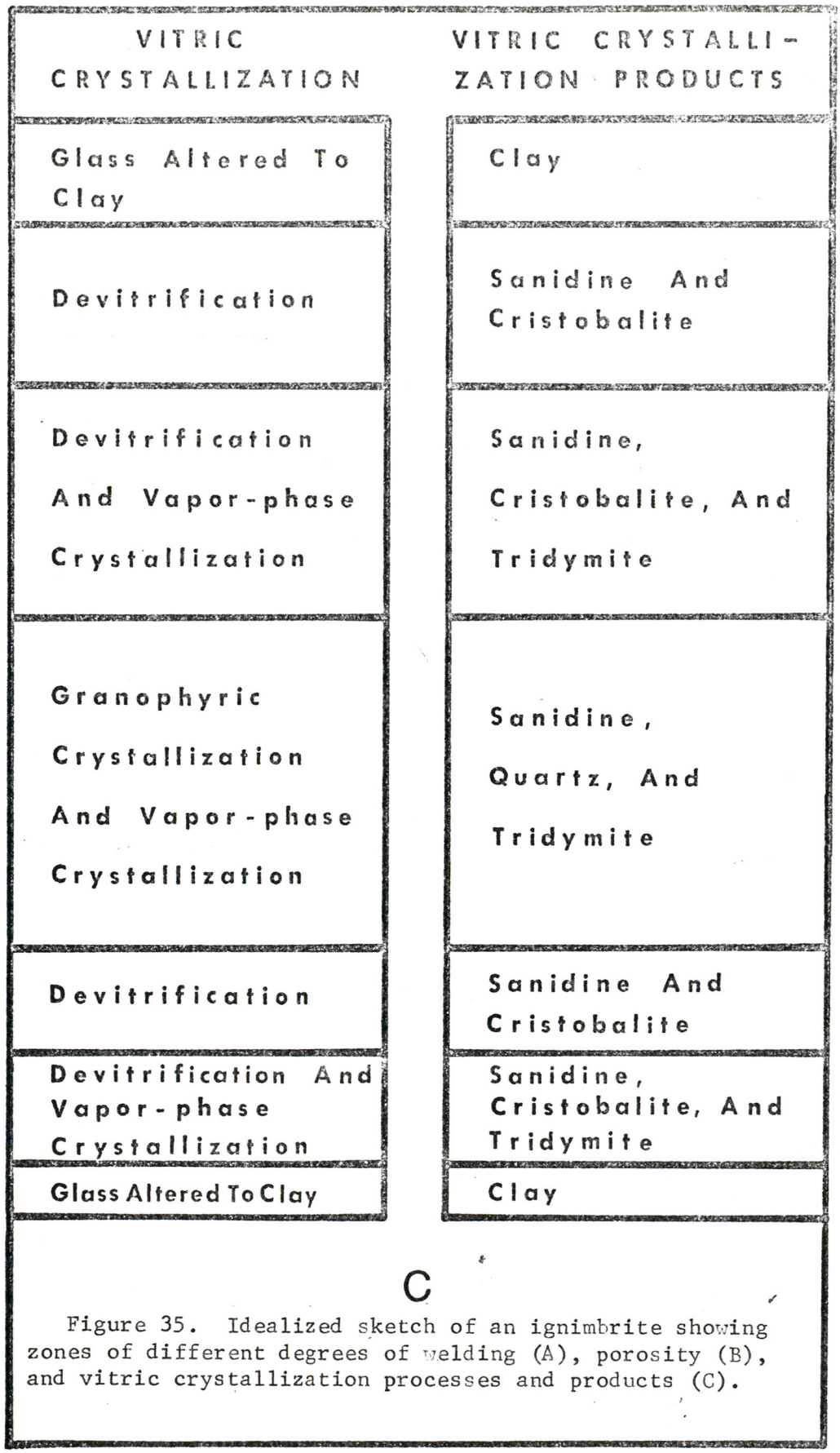

Figure 35. Idealized sketch of an ignimbrite showing zones of different degrees of welding (A), porosity (B), and vitric crystallization processes and products (C).

Unit 1 was relatively cool at the time of emplacement. The zone of greatest welding, which is only moderately welded, is high in the section. A relatively cool, viscous magma could also explain the large pumice content of about 33%.

The relict shards of Unit 1-A crystallized into spherulitic and axiolitic intergrowths of sanidine and cristobalite. The relict pumice lumps underwent granophyric crystallization to sanidine and quartz. Most of Unit 1-B underwent granophyric crystallization to sanidine and quartz. Vapor-phase crystallization of sanidine and tridymite occurred in the cavities throughout Unit 1. Upward in the section, the plagioclase and accessory phenocrysts increase slightly in abundance at the expense of sanidine (Table 8b). The variation possibly reflects a difference in composition between magma in the upper and lower levels of the magma chamber (Macdonald, 1972).

Units 2, 3, and 4

Units 2, 3, and 4 were emplaced in rapid succession as three separate flows; consequently the entire mass cooled as a single cooling unit (Fig. 36a, b, c, and d).

Unit 2 is 29 m thick and comprises about 69% of the cooling unit. The ignimbrite was relatively hot because a basal vitrophyre formed. A decrease in porosity occurs toward the top of Unit 2-B (Fig. 36b). This decrease in porosity was caused by the emplacement of Units 3 and 4 while Unit 2 was still undergoing compaction.

Unit 3 is about 9 m thick and constitutes about 23% of the cooling unit. Upward in the section but below the upper 3 m of the unit, there

Figure 36a. Zones of different degrees of welding for Units 2, 3, and 4, Sacramento, Chihuahua, Mexico. Unit 2-A is a basal vitrophyre where shards are intensely welded and pumice lumps are completely collapsed. In Unit 2-B and 3, moderate welding of shards occurred and pumice lumps are flattened but not completely collapsed. The lithics in Unit 4 are moderately welded and flattened and pumice lumps are flattened to varying degrees.

Figure 36b. Porosity curves for Units 2, 3, and 4, Sacramento, Chihuahua, Mexico. The low porosity of Unit 2-A (basal vitrophyre) is due to intense welding and compaction of shards and pumice lumps. Fractures are responsible for most of the porosity in Unit 2-A. The porosity of Unit 2-B decreases upward in the section. This trend is opposite that of a single flow and cooling unit. The shift from the normal trend of a single flow (Figure 35b) was due to load pressure (Units 3 and 4) being added before Unit 2-B was lithified. Unit 3 also shows a decrease in porosity from the center of the unit upwards in the section, but below the uppermost 3 m of the unit. This shift from the normal porosity trend of a single flow was due to load pressure (Unit 4) being added before Unit 3 was lithified. The increase in porosity in the upper 3 m of Unit 3 is probably due to an increase in lithic fragment content. Unit 4 has a normal porosity curve for the lower part of an ignimbrite.

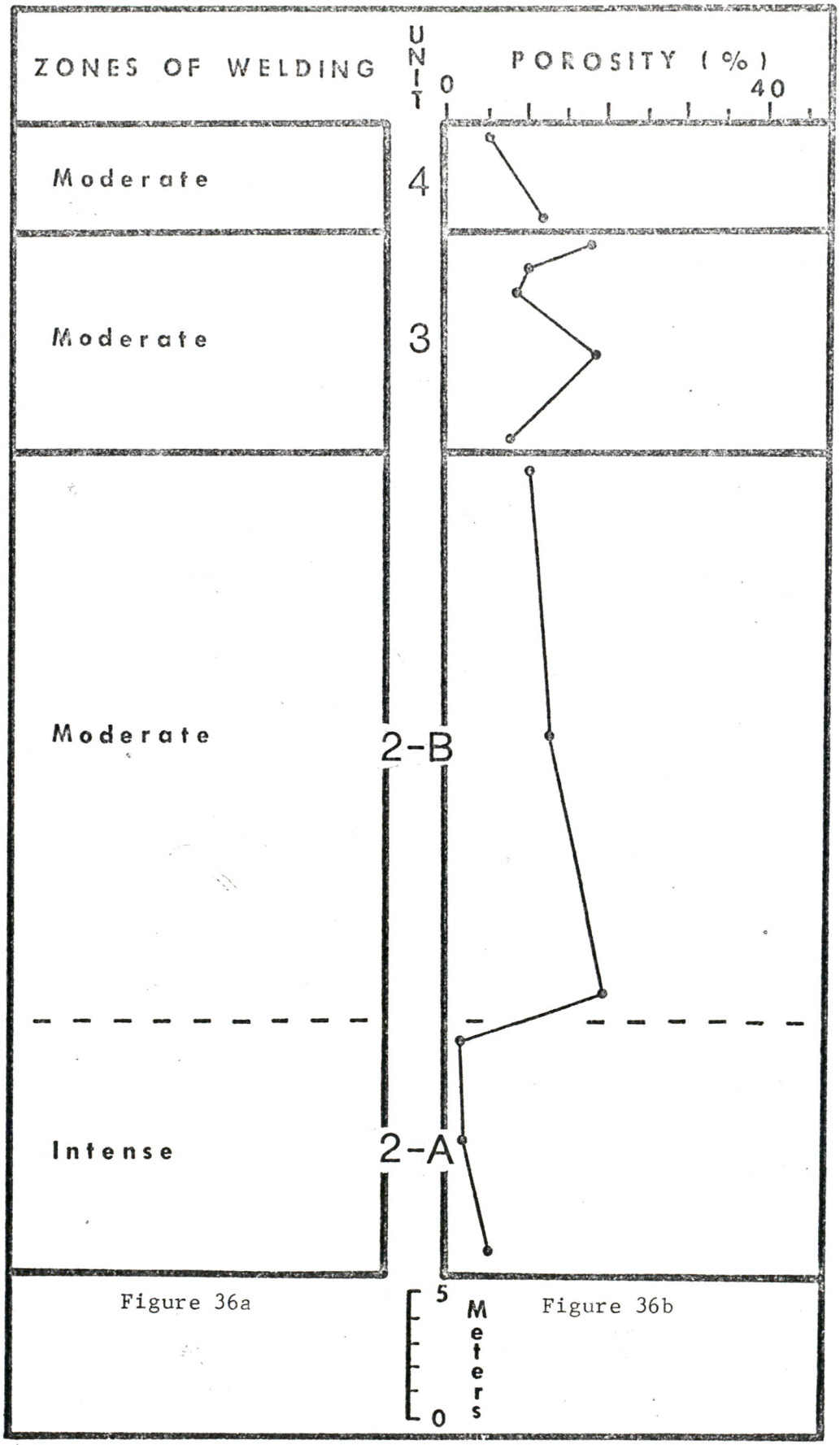

Figure 36a

Figure 36b

Figure 36c. Types of vitric crystallization of Units 2, 3, and 4, Sacramento, Chihuahua, Mexico. Unit 2-A devitrified into spherulitic structures of sanidine and cristobalite. The base of Unit 2-B underwent granophyric crystallization to sanidine and poikilitic quartz. The middle and upper parts of Unit 2-B and Unit 3 devitrified into axiolitic structures of sanidine and cristobalite. This zone also contains spherulites (sanidine and cristobalite), and sanidine and poikilitic quartz. Unit 4 is composed primarily of lithic fragments so the groundmass is not vitric (not applicable).

Figure 36d. Vapor-phase minerals of Unit 2, 3, and 4, Sacramento, Chihuahua, Mexico. The absence of vapor-phase minerals in Unit 2-A is due to the lack of pore space. Sanidine and/or tridymite are the major vapor-phase minerals in the other units.

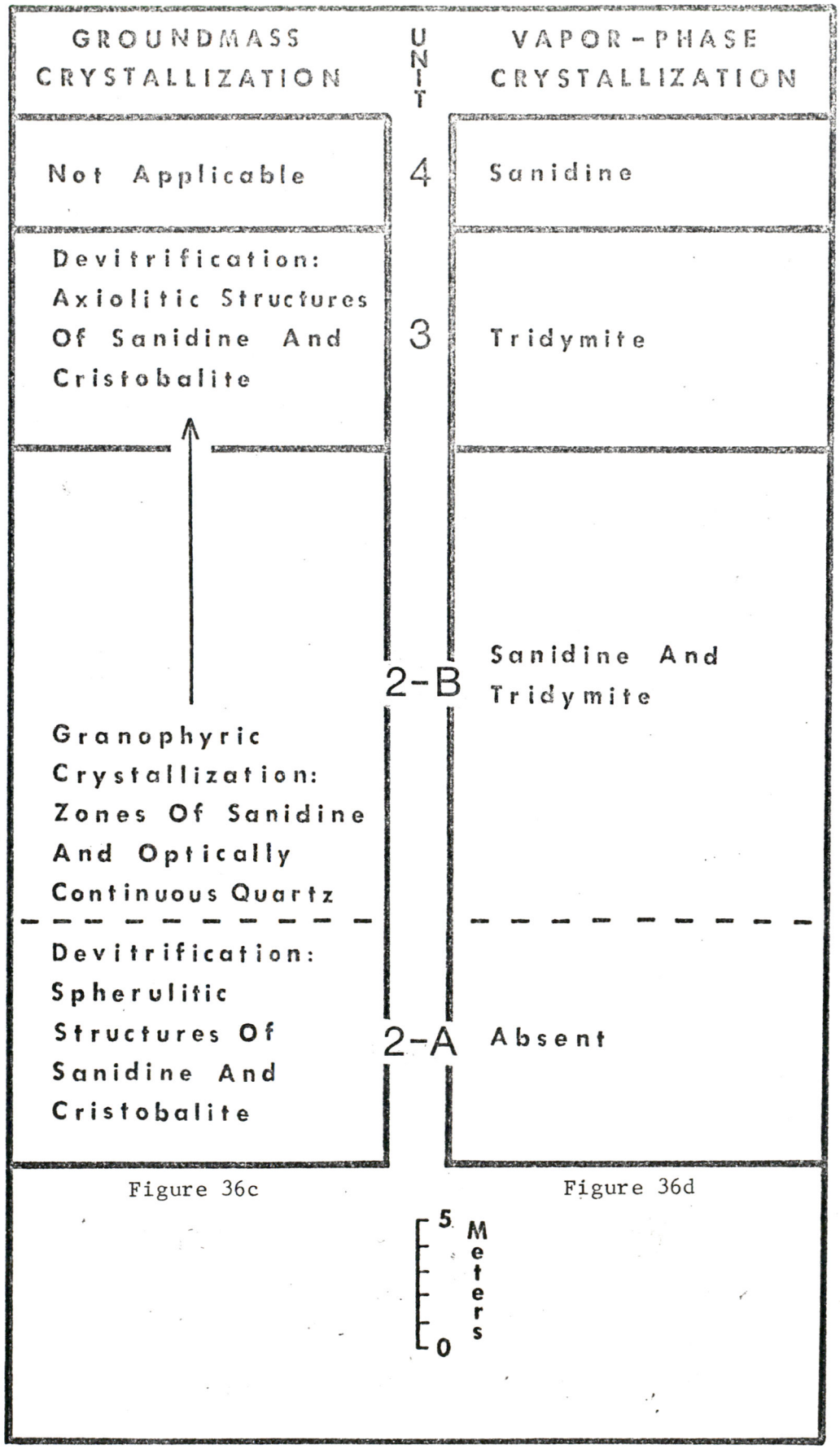

Figure 36c

Figure 36d

is a decrease in porosity from the middle to upper portions (Fig. 36b). The increase in porosity of the uppermost portion of Unit 3 is due to an increase in lithic fragments (Table 7) which are less compacted than shards and pumice lumps.

Unit 4 is 3 m thick and comprises about 8% of the cooling unit. It has a normal porosity curve (Fig. 36b) for the lower middle portion of a relatively thin ignimbrite that has been truncated by erosion. The base of Unit 4 lacks an unwelded portion because temperatures were high. However, the temperature was not sufficiently high to form a basal vitrophyre.

The partings separating Units 2, 3, and 4 were indurated by heat and gas activity. Succeeding flows scoured the surfaces over which they moved and picked up semi-consolidated and unconsolidated ash. Some of the phenocrysts, pumice, and shards of Unit 4 could have been derived from Unit 3 in this fashion.

The basal vitrophyre of Unit 2 exhibits well developed spherulites of sanidine and cristobalite (Fig. 36c). Directly above the vitrophyre, the slowest cooling zone (lower portion of Unit 2-B) developed complete granophyric crystallization to sanidine and poikilitic quartz. The sanidine and poikilitic quartz zone grades upward into a mixed zone of equidimensional grains, spherulites, and axiolitic growths of sanidine and cristobalite. Unit 4 is comprised primarily of lithic fragments and did not have an originally glassy matrix.

Vapor-phase crystallization in the basal vitrophyre of Unit 2 is limited to fractures because of the degree of compaction. Unit 2-B, Unit 3, and Unit 4 contain tridymite and sanidine vapor-phase crystals.

These formed due to the large amount of pore space (Fig. 36b) and because these zones were high in the original cooling unit (Fig. 36a).

Upward in the section, the cooling unit becomes richer in crystals and lithic fragments (Table 7). There is no change in the type of phenocrysts or lithic fragments. Unit 2 contains only 0.7% phenocrysts and 0.4% lithic fragments. It represents the major eruption of the cooling unit. After Unit 2 was erupted, the vent-fissure complex probably collapsed and filled with broken wall rock. Unit 3 contains 5% phenocrysts and 5% lithic fragments. It represents the second eruption of the cooling unit. The magma of Unit 3 was enriched in phenocrysts relative to the magma of Unit 2 and the lithic fragments were incorporated while the eruptive material passed through the vent-fissure complex. After Unit 3 was erupted, the vent-fissure complex probably collapsed again. Unit 4 contains 7% phenocrysts and about 70% lithic fragments. It represents the third and probably last eruption of the cooling unit. Unit 4 may contain no primary magma as shards; instead the lithic fragments, phenocrysts, pumice lumps, and shards simply occupied the vent-fissure complex at the time of a phreatic explosion. Unit 4 also derived semi-consolidated and unconsolidated ash, phenocrysts, and pumice lumps from the underlying unit due to the scouring action of the ash flow.

Unit 5

Unit 5 is a single flow and cooling unit. It was probably a small and relatively cool ash flow. The ignimbrite has an unwelded altered basal part which grades upward into a zone of moderate welding. The glassy matrix of the unwelded basal tuff was altered to a smectite-group

clay by ground water. The excess silica left over from the alteration is a possible source of botryoidal quartz that formed in cavities of Units 3 and 4. The zone of moderate welding probably marks the most intensely welded part of Unit 5 and is the most erosionally resistant portion. The glassy matrix devitrified to sanidine and cristobalite. Pumice lumps underwent granophyric crystallization to sanidine and quartz. Vapor-phase crystallization formed sanidine and tridymite crystals in pore space (Fig. 36d).

TECTONIC IMPLICATIONS

During the Laramide orogeny (late Cretaceous to late Eocene), calc-alkalic volcanism occurred along the western margin of the American plate (Lipman and others, 1972). McDowell and Keizer's (1977) lower volcanic complex of western Mexico was formed during this time. The Peñas Azules volcanics of the Majalca area are probably part of this lower volcanic complex.

According to Elston (1976), the Laramide orogeny was followed by an active stage of extension (late Eocene to Miocene) and a passive stage of extension from Miocene to present. The active stage of extension started with slower rates of subduction and changes in the direction of plate movement along the western edge of the American plate. Calc-alkalic to alkalic volcanism occurred during this period. High silica alkali rhyolites were formed by partial melting of sialic lithosphere (Elston, 1976). The plutons of high silica alkali rhyolite magma rose into the continental lithosphere that was free to rise vertically and stretch horizontally due to the relaxation of compressional forces (Elston, 1976). The late Eocene high silica alkali rhyolitic ignimbrites of the Sacramento area were probably erupted during this period. These rocks are located between the calc-alkalic igneous centers of western Mexico (Elston, 1976) and the alkalic igneous centers of western Texas (Barker, 1977), and can be considered intermediate in composition between calc-alkaline and alkaline.

The passive stage of extension began with the cessation of subduction along the western margin of the American plate (Elston, 1976).

Diapric masses of basaltic material rose into the continental lithosphere and were erupted to form fundamentally basaltic suites (McDowell and Keizer, 1977). Block faulting and epeirogenic uplift occurred during this period. The Oligocene ignimbrites of the main Sierra Madre Occidental may have been related to this period of relaxation following compression.

C O N C L U S I O N S

The welded vitric tuffs in the vicinity of Sacramento, Chihuahua, Mexico are classified as:

1) high silica rhyolites - silica contents are greater than 72%,
2) subaluminous/peralkaline rhyolites - the molecular ratio of alumina to soda + potash + lime is approximately one, and
3) alkali rhyolites - the rocks are composed of sanidine and SiO_2 polymorphs.

The ignimbrites were erupted during the active stage of extension (late Eocene to Miocene) which followed the Laramide orogeny (Elston, 1976). The rocks are located between the calc-alkalic igneous centers of western Mexico and the alkalic igneous centers of the west Texas region. The ignimbrites are intermediate in composition between the calc-alkalic igneous rocks of western Mexico and the alkalic igneous rocks of western Texas.

REFERENCES

Alba, L. A., and Chavez, R., 1974, K-Ar ages of volcanic rocks from the central Sierra Peña Blanca, Chihuahua, Mexico: Isochron/West, no. 10, p. 21-23.

Allman, M., and Lawrence, D. F., 1972, Geological laboratory techniques: Arco Publishing Co., New York, 335 p.

Barker, D. S., 1977, The northern Trans-Pecos Magmatic Province: An introduction and comparison with the Kenya Rift: in press, Geol. Soc. America Bull.

Bowen, N. L., and Tuttle, O. F., 1950, The system $NaAlSi_3O_8$ - $KAlSi_3O_8$ - H_2O: Jour. Geol., v. 58, p. 489-511.

Christiansen, R. L., and Lipman, P. W., 1972, Cenozoic volcanism and plate-tectonic evolution of the Western United States. II. Late Cenozoic: Phil. Trans. R. Soc. Lond., A. 271, p. 249-284.

Cook, E. F., 1965, Stratigraphy of Tertiary volcanic rocks in eastern Nevada: Nevada Bureau of Mines Report 11, 61 p.

DeFord, R. K., 1969, Some keys to the geology of northern Chihuahua: in New Mexico Geological Society 20th Field Conference Guidebook - The Border Region, Chihuahua and the United States, Cordoba, D. A., Wengerd, S. A., and Shomaker, J., eds., p. 61-65.

Elston, W. E., 1976, Tectonic significance of mid-Tertiary volcanism in the Basin and Range province: A critical review with special reference to southwestern New Mexico: in New Mexico Geological Society Special Publication No. 5 - Cenozoic volcanism in southwestern New Mexico, Elston, W. E., and Northrop, S. A., eds., p. 93-102.

Fisher, R. V., 1960, Proposed classification of volcanic rocks (abs.): Geol. Soc. America Bull., v. 71, p. 1864-1865.

Flanagan, F. J., 1967, U. S. Geological Survey silicate rock standards: Geochim. et Cosmochim. Acta, v. 31, p. 289-308.

Folk, R. L., 1974, Petrology of sedimentary rocks: Hemphill Publishing Co., Austin, Texas, 182 p.

Gall, D. G., 1975, The ignimbrites in the vicinity of Sacramento, Chihuahua, Mexico (abs.): Elisha Mitchell Scientific Soc. Jour., v. 91, p. 69.

Goddard, E. N., Trask, P. D., DeFord, R. K., Rove, O. N., Singewald, J. T., Jr., and Overbeck, R. M., 1963, Rock-color chart: Geological Soc. America, 11 p.

Hutchison, C. S., 1974, Laboratory handbook of petrographic techniques: Wiley-Interscience Publishing, John Wiley and Sons, New York, 527 p. Petrology

Jones, J. B., Nesbitt, R. W., and Slade, P. G., 1969, The determination of the orthoclase content of homogenized alkali feldspar using $\bar{2}01$ X-ray method: Mineral. Mag., v. 37, p. 489-496.

Lipman, P. W., Prostka, H. J., and Christiansen, R. L., 1972, Cenozoic volcanism and plate-tectonic evolution of the Western United States. I. Early and Middle Cenozoic: Phil. Trans. R. Soc. Lond., A. 271, p. 217-248.

Macdonald, G. A., 1972, Volcanoes: Prentice-Hall Inc., New Jersey, 510 p.

Mack, M., and Spielberg, N., 1958, Statistical factors in X-ray intensity measurements: Spectrochim. Acta, v. 12, p. 169-178.

McDowell, F. W., and Keizer, R. P., 1977, Timing of mid-Tertiary volcanism in the Sierra Madre Occidental between Durango City and Mazatlan, Mexico: in press, Geol. Soc. America Bull.

Mauger, R. L., 1975, Report to Consejo de Recursos, Mexico City, Mexico, 30 p.

_____, 1976, Chihuahua volcanic project; grant proposal to the Nat. Sci. Found.

Orville, P. M., 1963, Alkali ion exchange between vapor and feldspar phases: Amer. Jour. Sci., v. 261, p. 201-237.

_____, 1967, Unit-cell parameters of the microcline-low albite and the sanidine-high albite solid solution series: Amer. Mineralogist, v. 52, p. 55-86.

Ross, C. S., and Smith, R. L., 1961, Ash-flow tuffs: their origin, geologic relations, and identification: U. S. Geol. Survey Prof. Paper 366, 81 p.

Schmidt, R. H., Jr., 1973, A geographical survey of Chihuahua: Texas Western Press, El Paso, Texas, 63 p.

Shand, S. J., 1969, Eruptive rocks: their genesis, composition, classification, and their relation to ore-deposits with a chapter on meteorites: Hafner Publishing Co., New York, 488 p.

Smith, J. V., 1974, Feldspar minerals: crystal structure and physical properties, v. 1: Springer-Verlag Inc., New York, 627 p.

Smith, R. L., 1960, Zones and zonal variations in welded ash flows: U. S. Geol. Survey Prof. Paper 354-F, p. 149-159.

Sorensen, H., 1974, Introduction: in The alkaline rocks, Sørensen, H., ed.: Wiley-Interscience Publishing, John Wiley and Sons, New York, 622 p.

Spruill, R. K., 1976, The volcanic geology of the Rancho Peñas Azules area, Chihuahua, Mexico: unpublished Master of Science thesis, Dept. of Geology, East Carolina University, Greenville, N.C., 99 p.

Stanton, R. L., 1972, Ore petrology: McGraw-Hill Book Co., New York, 713 p.

Swanson, D. A., 1967, Yakima basalt of the Teton River area, south-central Washington (abs.): Geol. Soc. America Bull., v. 78, p. 1085.

Tuttle, O. F., and Bowen, N. L., 1958, Origin of granite in the light of experimental studies in the system $NaAlSi_3O_8$ - $KAlSi_3O_8$ - SiO_2 - H_2O: Geol. Soc. America Memoir 74, 153 p.